University of California
Santa Barbara

Quantum Chaos and Eigenstate Thermalization: Foundations and Implications

A dissertation submitted in partial satisfaction
of the requirements for the degree

Doctor of Philosophy
in
Physics

by

Fernando Iniguez

Committee in charge:

Professor Mark Srednicki, Chair
Professor Matthew Fisher
Professor Mark Sherwin

June 2023

The Dissertation of Fernando Iniguez is approved.

Professor Matthew Fisher

Professor Mark Sherwin

Professor Mark Srednicki, Committee Chair

June 2023

Quantum Chaos and Eigenstate Thermalization:

Foundations and Implications

by

Fernando Iniguez

To my parents and siblings.

Acknowledgements

I am profoundly grateful to my advisor, Mark Srednicki, who served as a true mentor throughout my journey. Under his guidance, I witnessed remarkable growth as a physicist, expanding my ability to think critically and creatively. His guidance extended beyond the realm of physics, encompassing valuable life advice. I deeply enjoyed all the stories we shared about our lives. The wisdom he imparted on me is a cherished treasure that I will carry with me for the rest of my life.

I had the privilege of collaborating with an exceptional group of individuals during my PhD journey, each of whom contributing to my growth and knowledge. I extend my gratitude to Sean McBride, Mark Srednicki, Chaitanya Murthy, Nicole Yunger Halper, and Arman Babakhani for their invaluable work and for the opportunity to work alongside them. Additionally, I am indebted to the brilliant physicists at UCSB, whose countless insightful conversations provided me with illuminating perspectives on problem-solving. Although their names are too numerous to mention, their collective wisdom has shaped my understanding of physics in profound ways.

I would like to express my appreciation to Matthew Fisher and Mark Sherwin for their roles as members of my thesis committee, guiding and overseeing my progress throughout the years. Furthermore, I am grateful to Richard Rains for helping me first develop my physics intuition during my time at Los Angeles Mission College, to Daniel Kasen for his valuable academic advice and encouragement, and to Barbara Jacak for her mentorship and the opportunity to be part of her research group while attending UC Berkeley. I am thankful for the generous funding provided by the National Science Foundation and the University of California, which has been instrumental in supporting my research endeavors.

I extend my deepest appreciation to my extraordinary friends and family who consistently offered words of support and were always there to lend a listening ear. Your presence was

indispensable to my achievements, and I am immensely grateful to each and every one of you. Above all, I want to express my heartfelt gratitude to my mother, father, sister, and brother for their unwavering love and endless encouragement. I consider myself incredibly fortunate to have such remarkable individuals in my life.

Curriculum Vitæ

Fernando Iniguez

Education

2023	Ph.D. in Physics (Expected), University of California, Santa Barbara.
2021	M.A. in Physics, University of California, Santa Barbara.
2018	B.A. in Physics, University of California, Berkeley.

Publications

1. C. Murthy, A. Babakhani, **F. Iniguez**, M. Srednicki, and N. Yunger Halpern, *Non-abelian eigenstate thermalization hypothesis*, Phys. Rev. Lett. 130 (Apr, 2023) 140402.
2. S. McBride and **F. Iniguez**, *Entanglement negativity transitions in chaotic eigenstates*, arXiv:2303.0001.
3. **F. Iniguez** and M. Srednicki, *Quantum fisher information for different states and processes in quantum chaotic systems*, arXiv:2304.0165.
4. **F. Iniguez** and M. Srednicki, *Microcanonical truncations of observables in quantum chaotic systems*, arXiv:2305.1570.

Abstract

Quantum Chaos and Eigenstate Thermalization:

Foundations and Implications

by

Fernando Iniguez

The eigenstate thermalization hypothesis (ETH) has been widely accepted as the mechanism by which isolated non-integrable quantum systems thermalize and has cemented itself as a cornerstone of quantum many-body physics. With advancements in technology enabling the creation of such systems, further exploration and theoretical development of ETH are necessary.

First, we expand ETH to the regime of isolated non-integrable quantum systems with non-Abelian conserved charges. We show that our extension, the non-Abelian eigenstate thermalization hypothesis, indeed predicts thermal expectation values of local observables, filling a crucial gap toward a more general framework.

We further investigate ETH's validity by examining the structure of observable matrix elements in the energy eigenstate basis. ETH-predicted matrix elements cannot be completely random and independent due to unrealistic consequences such as nonsensical results for the n-point correlation function of an observable. Nevertheless, assuming ETH, we discover a centered Jacobi ensemble distribution for the eigenvalue spectrum of a truncated observable operator in the energy basis. This analytical solution, converging to the Wigner semi-circle for small truncations, reinforces the intuitive notion that ETH applies within a limited energy window. Additionally, it serves as a benchmark for comparing numerical results, enabling the study of the correlations between energy eigenstates of a system.

Next, we delve into a critical inquiry: how can we differentiate between an energy eigen-

state conforming to ETH and a genuinely thermal density matrix? Quantum Fisher information (QFI) offers a theoretical tool that distinguishes between these two states. However, the choice of state preparation protocol significantly influences QFI. To address this, we systematically examine the resulting QFI for both an energy eigenstate and a thermal density matrix across diverse experimental protocols.

Lastly, we explore entanglement negativity in the context of chaotic eigenstates. We study phase transitions in a simplified model of entanglement negativity to facilitate analytical tractability. This allows us to establish conditions on the volume fractions for a tripartite system where predictions for the entanglement negativity based on ETH align or deviate from thermal predictions.

Contents

Curriculum Vitae **vii**

Abstract **viii**

1 Introduction **1**
1.1 Permissions and Attributions 6

2 Non-Abelian Eigenstate Thermalization Hypothesis **7**
2.1 Introduction to Quantum Chaos and Eigenstate Thermalization 7
2.2 Non-Abelian Conserved Charges 10
2.3 Non-Abelian ETH 12
2.4 Thermal and Quantum Predicition for $M = O(N)$ 14
2.5 Discussion and Conclusions 25

3 Microcanonical Truncations of Observables in Quantum Chaotic Systems **27**
3.1 Introduction 28
3.2 Microcanonical Truncations of an Observable Operator 29
3.3 Conclusions 34

4 Quantum Fisher Information for Different States and Processes in Quantum Chaotic Systems **37**
4.1 Introduction 38
4.2 Quantum Fisher Information 39
4.3 Experimental protocols 41
4.4 An Even Briefer Review of ETH 46
4.5 Computing QFI 47
4.6 Conclusions 51

5 Entanglement Negativity Transitions in Chaotic Eigenstates **53**
5.1 Introduction 53
5.2 Entanglement Negativity 55
5.3 Negativity Phase Transitions 66

5.4 Discussion 85

6 Future Directions **86**

Bibliography **90**

Chapter 1

Introduction

The concept of macroscopic thermalization is intuitive to everyone. Everyone has seen a beer, coffee, or ice cream left unattended for too long undergo thermalization. The beer warms up, the coffee cools down, and the ice cream melts. These changes occur due to external influences from the environment. This is thermalization. But what if the beer were completely isolated from the rest of the universe? Would it still undergo thermalization? At its core, the beer is comprised of constituent quantum particles. When considering the beer as a quantum mechanical system, the question arises: Do isolated quantum systems thermalize[1]? The answer to this fundamental question is crucial for our understanding of physics, as it bridges the gap between quantum mechanics and statistical mechanics. The answer, however, is not straightforward. To comprehend it, we delve into a historical review, which encompasses decades of conjectures, ansatzs, and a wealth of numerical and empirical evidence. Having understood the answer to this question opens a rich avenue of research directions, which we explore in this thesis.

While studying atomic nuclei in the 1950's, Wigner had the ingenious idea of considering the nuclei as a quantum mechanical system whose hamiltonian resembles a random matrix

[1] In this thesis thermalization refers to a system that can be described by a "traditional" thermal ensemble (such as the canonical ensemble). This is different than a system reaching *equilibrium*, which they all do, and will be explained shortly.

[1]. This idea was reinforced by energy level spacing statistics of atomic nuclei matching eigenvalue statistics predicted by random matrix theory (RMT). After some refinement, and classification using different types of random matrices by Dyson [2], the eigenvalue statistics of these systems would be named Wigner-Dyson statistics. Indeed Wigner-Dyson statistics were proven to hold for nuclear energy levels [3].

In an attempt to more generally describe which systems should exhibit Wigner-Dyson statistics, Bohigas, Giannoni, and Schmit conjectured that a quantum mechanical system with a hamiltonian whose classical counterpart is chaotic should obey the spectral properties predicted by RMT [4]. Backed by numerical evidence, this phenomena became known as *quantum chaos*. Even though the BGS conjecture was upheld by many single-particle quantum examples that had classic counterparts [5, 6, 7], it also held for quantum many-body systems that do not necessarily have a classical counterpart [8, 9]. A more encompassing phrase would be that *non-integrable quantum systems* obey the properties predicted by RMT, since that would encompass the systems detailed by the BGS conjecture and systems that do not have a classic counterpart. However, this also proves to be too general of a statement for reasons explained further below. To maintain specificity and accuracy while still incorporating historical nomenclature, it is customary to say that *most* non-integrable quantum systems have the properties predicted by quantum chaos.

The question of which isolated quantum systems thermalized was answered independently by Deutsch and Srednicki and relied on the aforementioned history. Deutsch showed this by introducing a random matrix perturbation to an integrable system, effectively making the system non-integrable, and showing that the average-time quantum expectation value of an observable approximated the microcanonical result [10], and by extension the canonical ensemble (thermal) expectation value[2]. Srednicki answered this question[3] with the use of Berry's con-

[2]This extension is made by the equivalence of thermodynamic ensembles in the thermodynamic limit

[3]Although I know for a fact Mark wasn't thinking about isolated quantum beers.

jecture, which states that the energy eigenstates of a quantum system whose classical counter part is chaotic can be written as the superposition of gaussian random waves [11]. With a single energy eigenstate that conforms to Berry's conjecture, Srednicki reproduced a Boltzmann, Bose-Einstein, and Fermi-Dirac distribution for the momentum of each constituent particle of a hard-sphere gas, effectively linking quantum mechanics and quantum statistical mechanics [12]. The phenomena of a single energy eigenstate reproducing thermal results for a local observable was further developed into the eigenstate thermalization hypothesis (ETH) which is an ansatz for the structure of physically observable matrix elements in the energy eigenbasis of quantum chaotic systems [13]. When posing the question of which type of isolated quantum systems thermalize, one could expect any of the following responses: those that obey quantum chaos, ETH, or most non-integrable systems. For the rest of this thesis we use these three interchangeably.[4]

To this end, it became obvious that isolated integrable systems do not thermalize. Integrable systems have energy level spacing statistics that follow a Poisson distribution and not any of the ones predicted by quantum chaos. Their internal dynamics are more tractable due to an large (extensive with degrees of freedom) number of conserved quantities. Instead, integrable systems equilibrate to a more complicated generalized Gibbs ensemble (GGE) [14]. It is also known that non-integrable systems can exhibit various phenomena such as many body localization, quantum many-body scars, and Hilbert space fragmentation, which can either strongly or weakly violate ETH, thus obstructing thermalization [15, 16, 17].

The answer to whether or not an isolated quantum system thermalizes was fundamental but seemingly theoretical; however, it became more relevant with the advancement of technology. In a seminal experiment by Weiss et al., an integrable system of trapped one-dimensional Bose gases comprised of ^{87}Rb formed a quantum Newton's cradle where thermalization was not observed [18]. The experimental possibility to create isolated non-integrable quantum systems

[4]For brevity, "most non-integrable" and "non-integrable" will be used interchangeable henceforth.

motivated an exploration for other properties these systems may have, and how the resulting phenomena can be used in applicable fields of research such as quantum computing. On the theoretical research side, quantum information theory, black hole physics, and many other fields have had illuminating results because of the understanding of quantum chaotic systems. ETH proves to be a powerful tool in solving for properties of otherwise intractable systems, and it is crucial to further our understanding of it. In this thesis we explain eigenstate thermalization and quantum chaos, expand on their foundational understanding, and explore the implications they have on non-integrable quantum systems.

In Chapter 2 we briefly review ETH, now a cornerstone of many-body physics, and extend it to the general case of a system with non-Abelian conserved charges. Reproducing thermal results via the ETH ansatz had been resolved for Abelian systems which have no degeneracies. The last gap in the literature is the case of a system which has energy degeneracies due to conserved non-commuting charges. In our extension, the *non-Abelian Eigenstate Thermalization Hypothesis*, we find that for sufficiently feasible conditions, thermal and quantum expectation values may differ by an $O(\frac{1}{N})$ term, agreeing with standard ETH. While this result was derived for a specific system, we expect it to hold for most generic non-integrable systems, and it suffices as a true extension of the ETH to the non-Abelian case.

In Chapter 3 we once again probe the validity of the ETH and expand its foundational understanding. ETH instructs us to think of an observable having random matrix properties for a suitably small energy eigenspace range. The question of *how small* of an energy range one should consider is a topic of discussion. Furthermore, observable matrix elements cannot be completely random and independent due to unrealistic consequences, such as the n-point time correlation function of an observable only depending on the 2-point correlation function. Nevertheless, we take ETH at face value for exploratory purposes. For a single-spin-component operator transformed into the energy eigenbasis via a random unitary transformation, we present an analytical form of the spectra after performing truncations on it. This is a toy model as the

unitary which takes you into the energy basis should encode true correlations between energy states and could not possibly be fully random. However, this result still proves to be very illuminating. The derived generalized form for the eigenvalue spectra is that of a centered Jacobi ensemble. For a very small truncation size the spectra has an analytic convergence to random matrix statistics appearing in the form of a Wigner semicircle. We provide a quantitative criterion for the truncation size at which the distribution *definitely* ceases to be a Wigner semicircle. At half the Hilbert space truncation size, a phase transition is observed. For energy truncations greater than half the Hilbert space dimension, the spectra of a centered Jacobi ensemble is observed along with Dirac deltas along the original eigenvalues of the observables. We present numerical results which agree with the theory. These results fortify the intuitive notion of when ETH is expected to hold, and serve as a benchmark for comparing numerical results in true physical systems.

In Chapter 4 we explicate the possibility of distinguishing between energy eigenstates that obey ETH and truly thermal density operators. Since chaotic eigenstates self-thermalize it begs the question if an experimenter can distinguish between one of these states and a truly thermal state. From a theoretical point of view, Quantum Fisher information (QFI), a quantity determined by how a system is prepared, differs between the two and thus serves as a mechanism to distinguish them. QFI of a chaotic eigenstate and thermal state are cataloged for different experimental processes. These results also have implications for quantum metrology. From an experimental point of view, QFI can be measured indirectly through the dynamic susceptibility of a system that has thermalized and bounds the uncertainty of an ideal measurement by the Cramér-Rao bound.

In Chapter 5 we explore the Rényi negativities and entanglement negativity of quantum chaotic systems. Entanglement negativity proves to be a feasibly computable quantity to diagnose entanglement in generic bipartite systems. A brief review of entanglement negativity is presented, followed by a model-specific analysis through the lens of chaotic eigenstates. The

difference between the canonical and chaotic eigenstate Rényi negativities are calculated in an effort to identify the regimes in which these quantities are self-averaging (when ETH holds). Various phase transitions are presented in a particular phase space region of interest for a pure state tripartite system. In particular, it is found that the even and odd Rényi negativities, and their analytic continuations, entanglement negativity, and partially transposed entropy, respectively, satisfy ETH depending on the volume partitioning of the three subsystems.

In conclusion, Chapter 6 talks about the implications of the work presented here as we explore potential avenues for future work.

1.1 Permissions and Attributions

The content of Chapter 2 is the result of a collaboration with Chaitanya Murthy, Arman Babakhani, Mark Srednicki, and Nicole Yunger Halpern, and has previously appeared in Physical Review Letters [19].

Chapter 2

Non-Abelian Eigenstate Thermalization Hypothesis

The eigenstate thermalization hypothesis (ETH) explains why chaotic quantum many-body systems thermalize internally if the hamiltonian lacks symmetries. If the hamiltonian conserves one quantity ("charge"), ETH implies thermalization within a charge sector—in a microcanonical subspace. But quantum systems can have charges that fail to commute with each other and so share no eigenbasis; microcanonical subspaces may not exist. Furthermore, the hamiltonian will have degeneracies, so ETH need not imply thermalization. In this chapter, we briefly review ETH and adapt it to non-commuting charges by positing a non-Abelian ETH and invoking the approximate microcanonical subspace introduced in quantum thermodynamics.

2.1 Introduction to Quantum Chaos and Eigenstate Thermalization

Quantum chaos predicts thermalization by use of Berry's conjecture, which states that the eigenstates of a quantum chaotic system can be written as the superposition of plane waves

with a fixed wavelength determined by the energy of that specific eigenstate and with gaussian random amplitudes and random phases [11]. Berry's conjecture reproduces a Boltzmann, Bose-Einstein, and Fermi-Dirac distribution for particles. It also shows that a single eigenstate predicts a thermal distribution for the expectation value of a local observable [12]. This phenomenon, in which a single energy eigenstate reproduces thermal behavior for an observable, is known as eigenstate thermalization. The field of quantum chaos has widely accepted the moniker eigenstate thermalization hypothesis (ETH) and uses it when referring to systems that obey certain properties predicted by quantum chaos.

The foundation of ETH is based on the ansatz that quantum chaotic systems have observable matrix elements with the form of

$$A_{ij} = \mathcal{A}(E)\delta_{ij} + e^{-S(E)/2} f(E,\omega) R_{ij} \tag{2.1}$$

in the energy basis [13]. Here $S(E)$ is the standard thermodynamic entropy of the system at a specified energy E and $\omega = E_i - E_j$. The matrix R_{ij} is gaussian random and has the properties $\overline{R_{ij}} = 0$, $\overline{R_{ij}R_{kl}} = \delta_{ik}\delta_{jl}$, and $R_{ij} = R^*_{ji}$ by the hermiticity of A. $\mathcal{A}(E)$ and $f(E,\omega)$ are real, smooth functions of their arguments, with the latter being positive and an even function of ω.

One can derive thermal behavior using Eq. (2.1) by looking at the quantum time expectation value of an observable in a generic quantum state,

$$A_t \equiv \langle\psi(t)|A|\psi(t)\rangle = \sum_{ij} c_i^* c_j e^{i(E_i - Ej)t} A_{ij}. \tag{2.2}$$

Taking an infinite time average of Eq. (2.2) yields

$$\bar{A} = \sum_i |c_i|^2 A_{ii}, \tag{2.3}$$

where the non-degeneracy of energies has been assumed. We know from statistical mechanics

that at equilibrium thermal averages have small fluctuations. So, for all intents and purposes, $\bar{A} = \langle A \rangle_T$ where $\langle A \rangle_T$ is the thermal average, $\mathrm{Tr}(e^{-\beta H} A)/Z$, of an observable. The connection comes back to quantum chaos when one inputs matrix elements of the form seen in Eq. (2.1) into Eq. (2.3). The link between quantum mechanics and statistical mechanics is encoded in $\mathcal{A}$ by the relationship

$$\mathcal{A}(E) = \langle A \rangle_T + \mathcal{O}(N^{-1}) + \mathcal{O}(e^{-S/2}). \tag{2.4}$$

This gives a thermal prediction for an observable A in an initial quantum state that satisfies ETH. When removing the assumption of non-degeneracy, linking quantum chaos to thermalization via ETH becomes more involved.

Understanding probes of quantum chaos is a heavily studied topic [20, 21, 22, 23]. Traditionally, one looks at the eigenvalue statistics of the hamiltonian to see if the underlying system obeys ETH. This is due to the BGS conjecture which claims that quantum hamiltonians whose classical counterparts are chaotic have eigenstatistics predicted by random matrix theory (RMT) [4]. Because of this, RMT and quantum chaos have become two closely-knit fields. The energy level spacings of quantum chaotic systems are predicted to follow one of three Wigner-Dyson distributions which are derived from random matrices [2]. Checking the level spacings is often a daunting task. Instead, a more universally applicable method is to check the ratio of level spacings. In this case, the three distributions are given by

$$P_W(r) = \frac{1}{Z_B} \frac{(r + r^2)^\beta}{(1 + r + r^2)^{1+\frac{3}{2}\beta}} \tag{2.5}$$

where r is given by the ratio of consecutive level spacings, $(e_3 - e_2)/(e_2 - e_1)$, and a normalization factor Z_B [24]. The Dyson index, β, is system dependent and takes on the values 1, 2, and 4 for hamiltonians that are real (GOE), complex (GUE), or quaternionic (GSE), respectively.

Recovering Wigner-Dyson statistics in a system with no symmetries is straightforward. In

the case of Abelian symmetries it is a bit more subtle. These symmetries lead to the eigenbasis of a chaotic hamiltonian taking the form $\{|r, a; i\rangle\}$ where r runs through the number of symmetries, a labels the state within a given multiplet and i labels the different multiplet [25]. The matrix elements

$$\langle r, a, i|H|r', a', i'\rangle = \delta_{rr'}\delta_{aa'}H^{(r)}_{ii'} \tag{2.6}$$

indicate that this matrix element is zero across different sectors but illuminates nothing about the matrix elements within sectors. By looking at $H^{(r)}_{ii'}$, one can recover energy level distributions predicted by Eq. (2.5). Without looking in the appropriate basis (sectors) one would get a mixed statistics by looking at uncorrelated $H^{(r)}_{jj'}$ and $H^{(r')}_{ii'}$. This results in the known technique of looking within charge sectors to retrieve Wigner-Dyson statistics of a hamiltonian with Abelian symmetries. For Abelian conserved charges there will generically be no energy degeneracies and one can use the same arguments to get the same results as in Eq. (2.4). Hence, ETH still accurately predicts the behavior of systems with Abelian symmetries present. With the Abelian symmetry case treated, the last case needing to be bridged in the context of ETH is the most general, the case of non-Abelian conserved charges.

2.2 Non-Abelian Conserved Charges

Here we bridge the gap between ETH and conserved non-commuting charges. As previously explained, when Abelian symmetries are present one must look at sectors of the completely symmetry-factorized hamiltonian in order to get thermal predictions from ETH. This is possible because Abelian symmetries share an eigenbasis in which all symmetries can be resolved. However, this is not the case for non-Abelian symmetries. No simultaneous basis exists where all charges can be simultaneously diagonalized. Hence, we cannot say there is a basis for which matrix elements of observables have the form predicted by ETH. To circumvent this

we invoke the work of [26] which claims that there is an approximate microcanonical subspace which generalizes a microcanonical subspace for non-commuting charges. In this approximate microcanonical subspace there is eigenbasis which simultaneously diagonalizes our originally non-commuting charges by looking at a limiting case where they essentially commute[1].

Another subtlety arises when attempting to compare whatever form of ETH is derived to a proper thermal state as was done previously with a canonical ensemble. In order to compare an ETH-like result we need to know what thermal ensemble we expect our system to thermalize to. Relying on approximate microcanonical subspaces, systems with non-commuting conserved charges are stated to reach a non-Abelian thermal state with the form

$$\rho_{\text{NATS}} = e^{-\beta(H-\sum_a \mu_a Q_a)}/Z \tag{2.7}$$

where β and the μ_a take on the usual roles of effective chemical potentials defined by their conjugate observable's expectation value, $\langle Q_a \rangle = \text{Tr}(Q_a \rho_{\text{NATS}})$ [27]. We note the similarities of Eq. (2.7) to the form of a generalized Gibbs ensemble, which integrable quantum systems with commuting charges [14] equilibrate to, but point out their internal dynamics differ.

In order to find an answer, we consider a model which has properties that can make the problem tractable. More specifically, we consider a rotationally invariant system of N spin-$\frac{1}{2}$ qubits whose three components of angular momentum are conserved, i.e., $[H, S_{a=x,y,z}] = 0$. Of course the charges, namely the S_a, do not commute with each other, hence they are non-Abelian conserved charges. This introduces a conserved $\vec{S}^2$ observable. The system considered must be non-integrable such that the rules of quantum chaos hold, and must preserve the rotational symmetry of the system. An example of such a hamiltonian with the desired properties is a nearest-neighbor interaction between spins with varying interaction strength J_i, where the spread of interaction strengths, ΔJ, is not large enough to cause many-body localization [15].

[1] This is valid in the thermodynamic limit, which is the case we treat here.

The system has a shared eigenbasis for H, S_z and $\vec{S}^2$ given by $\{|\alpha, m_\alpha\rangle\}$ with the following eigenvalues:

$$H|\alpha, m_\alpha\rangle = E_\alpha|\alpha, m_\alpha\rangle \tag{2.8}$$

$$\vec{S}^2|\alpha, m_\alpha\rangle = s_\alpha(s_\alpha+1)|\alpha, m_\alpha\rangle, \quad \text{and} \tag{2.9}$$

$$S_z|\alpha, m_\alpha\rangle = m_\alpha|\alpha, m_\alpha\rangle, \quad \text{wherein} \tag{2.10}$$

$$m_\alpha = -s_\alpha, -s_\alpha+1, ..., s_\alpha \tag{2.11}$$

and begins in a normalized initial state

$$|\psi(t=0)\rangle = \sum_{\alpha, m_\alpha} c_{\alpha, m_\alpha}|\alpha, m_\alpha\rangle. \tag{2.12}$$

The system has energy $\langle H\rangle = E = O(N)$, $\langle S_z\rangle = M$, and we orient the system z-axis with $\langle\vec{S}\rangle$ so that the other non-commuting charges have expectation values $\langle S_{x,y}\rangle = 0$. The charges' variances are bounded by

$$\text{var}(H) \leq O(N), \tag{2.13}$$

$$\text{var}(S_z) \leq O(N), \quad \text{and} \tag{2.14}$$

$$\text{var}(S_{x,y}) \leq O(N) \tag{2.15}$$

which is within the realm of yielding physically significant measurements.

2.3 Non-Abelian ETH

At this point, if one tried to naïvely apply ETH for any observable and use the form of Eq. (2.1) they would not capture the non-Abelian nature of the system. The case of non-commuting charges encodes more information into observable matrix elements and so the orig-

inal ETH ansatz must be modified to accommodate for this. A way to see this is by making use of the fact that every observable is a linear combination of the irreducible spherical tensor operators, $T_q^{(k)}$, where k is an integer and denotes tensor rank and q is an integer amount of charge the operator imparts on an energy eigenstate and runs from $-k$ to k [28].
Some important commutation relations of use for our current problem are $[S_z, T_q^k] = qT_q^k$ and $[S_\pm, T_q^{(k)}] = \sqrt{(k \mp q)(k \pm q + 1)}T_{q\pm1}^{(k)}$, where $S_\pm$ are the standard raising and lowering operators. In the context of our system, a single site spin component, s_z^i, is a $T_0^{(1)}$ operator and the site ladder operators, $s_\pm^i$, are $T_{\pm1}^{(1)}$ operators.

For this work we focus on operators that are K-local. In other words, their operator norms are upper bounded by K where K is $O(1)$. Every K-local observable equals a linear combination of $T_q^{(k)}$'s whose $k \leq K$.

With the proper approach we can now encode the relevant information produced by conserved non-commuting charges into the ETH ansatz for observable matrix elements. Decomposing observables into spherical tensors and calculating their expectation value in the energy eigenbasis, one finds a recollection to the Wigner-Eckart theorem. Namely,

$$\langle \alpha, m_\alpha | T_q^{(k)} | \alpha', m_{\alpha'} \rangle = \langle s_\alpha, m_\alpha | s_{\alpha'}, m_{\alpha'}; k, q \rangle \langle \alpha || T^{(k)} || \alpha' \rangle, \tag{2.16}$$

where $\langle s_\alpha, m_\alpha | s_{\alpha'}, m_{\alpha'}; k, q \rangle$ are the well known Clebsch-Gordan coefficients. Note that the Clebsch-Gordan coefficients are a general statement on looking at charge sectors.

We now assume that the reduced matrix element $\langle \alpha || T^{(k)} || \alpha' \rangle$ obeys what we call non-Abelian ETH. As in traditional ETH, we define the average energy $\mathcal{E} = \frac{1}{2}(E_\alpha + E_{\alpha'})$, the energy difference $\omega = E_\alpha - E_{\alpha'}$, and the matrix $R_{\alpha\alpha'}$ as normally done. Due to our conserved charges our system can only explore a specified surface on phase space. Thus, we now define the average spin quantum number $\mathcal{S} = \frac{1}{2}(s_\alpha + s_{\alpha'})$ and the difference $\nu = s_\alpha - s_{\alpha'}$. The observable

$T_q^{(k)}$ obeys non-Abelian ETH if, for smooth, real functions $\mathcal{T}^{(k)}(\mathcal{E},\mathcal{S})$ and $f_\nu^{(k)}(\mathcal{E},\mathcal{S},\omega)$,

$$\langle\alpha||T^{(k)}||\alpha'\rangle = \mathcal{T}^{(k)}(\mathcal{E},\mathcal{S})\delta_{\alpha,\alpha'} + e^{-S_{th}(\mathcal{E},\mathcal{S})/2} f_\nu^{(k)}(\mathcal{E},\mathcal{S},\omega) R_{\alpha\alpha'}. \tag{2.17}$$

We label this equation non-Abelian ETH.

A few comments are in order about Eq. (2.17). We note the lack of dependence on $m_{\alpha,\alpha'}$. As seen in the LHS of Eq. (2.17) there is no m dependence, therefore the RHS cannot have a dependence on m. The dependence on $\mathcal{S}$ is deduced, as the non-Abelian symmetry can only be encoded by it. The deduction is made by considering the case where S_z is conserved but not $S_{a=x,y}$. In this case one could insert Eq. (2.17) into Eq. (2.16) and retrieve traditional ETH, where the Clebsch-Gordan coefficients just enforce charge conservation of M in the matrix elements of an operator, and $\mathcal{S}$ reduces to M by $|\vec{S}| = \sqrt{S_z^2 + S_x^2 + S_y^2}$. Hence, the non-Abelian nature is encoded by $\mathcal{S}$.

2.4 Thermal and Quantum Predicition for $M = O(N)$

Employing the help of Eq. (2.7), we expect our system to thermalize to a non-Abelian thermal state

$$\rho_{\text{NATS}} = \frac{1}{Z} e^{-\beta(H-\mu S_z)} \tag{2.18}$$

which we use to derive a thermal expectation of the spherical tensor operators:

$$\langle T_q^{(k)}\rangle_{\text{th}} = \text{Tr}(T_q^{(k)}\rho_{\text{NATS}}) = \frac{1}{Z}\sum_{\alpha,m_\alpha} e^{-\beta(E_\alpha-\mu m_\alpha)}\langle s_\alpha, m_\alpha|s_\alpha, m_\alpha; k, q\rangle \mathcal{T}^{(k)}(E_\alpha, s_\alpha). \tag{2.19}$$

This yields 0 if $q \neq 0$, so

$$\langle T_q^{(k)}\rangle_{\text{th}} = \frac{\delta_{q,0}}{Z}\sum_{\alpha,m_\alpha} e^{-\beta(E_\alpha-\mu m_\alpha)}\langle s_\alpha, m_\alpha|s_\alpha, m_\alpha; k, 0\rangle \mathcal{T}^{(k)}(E_\alpha, s_\alpha). \tag{2.20}$$

Taking the time-averaged expectation value in our time-evolved initial quantum state of a spherical tensor for any general k and q gives

$$\langle T_q^{(k)} \rangle_t = \sum_{\alpha,\alpha',m_\alpha,m_{\alpha'}} C^*_{\alpha,m_\alpha} C_{\alpha',m_{\alpha'}} e^{i(E_\alpha - E_{\alpha'})t} \langle s_\alpha, m_\alpha | T_q^{(k)} | \alpha', m_{\alpha'} \rangle. \tag{2.21}$$

Taking the infinite-time average and applying the non-Abelian ETH ansatz results in

$$\overline{\langle T_q^{(k)} \rangle_t} = \sum_{\alpha,m_\alpha} C^*_{\alpha,m_\alpha+q} C_{\alpha,m_\alpha} \langle s_\alpha, m_\alpha + q | s_\alpha, m_\alpha; k, q \rangle \mathcal{T}^{(k)}(E_\alpha, s_\alpha) \tag{2.22}$$

where the off-diagonal terms have vanished due to dephasing over an infinite time.

Up until this point, the conserved quantity M was never specified and the arguments were general. To determine whether thermalization, or any thermalization altering effect, results from non-Abelian conserved charges, we must look at different scaling regimes for M. We restrict ourselves to an extensive M but make some comments in the conclusion section regarding other scalings.

For $q = 0$, the thermal average (2.20) and infinite-time average (2.22) take on the similar form of

$$\langle T_0^{(k)} \rangle_p = \sum_{\alpha,m_\alpha} p_{\alpha,m_\alpha} \langle s_\alpha, m_\alpha | s_\alpha, m_\alpha; k, 0 \rangle \mathcal{T}^{(k)}(E_\alpha, s_\alpha). \tag{2.23}$$

In the infinite-time averaged case the probability distribution is that of the diagonal ensemble, $\{|C_{\alpha,m_\alpha}|^2\}$, and in the thermal average the distribution is $\{e^{-\beta(E_\alpha - \mu m_\alpha)}/Z\}$.

For thermal probabilities it is typical to expected the moment condition

$$\langle (E_\alpha - E)^a (m_a - M)^b (s_\alpha - M)^c \rangle_p \leq O(N^{a+b+c-1}) \forall (a,b,c) \in \mathbb{Z}^3_{\geq 0} \backslash (0,0,0). \tag{2.24}$$

This can be seen via Laplace's method and the conditions $E = O(N)$ and $M = O(N)$. It is not so easily seen that the diagonal ensemble yields the same moment condition.

2.4.1 Diagonal Ensemble Moment Condition

To examine corrections to thermal predictions from non-Abelian ETH, the moment conditions for E, M, and S must be derived in the diagonal ensemble. To do this we make use of the extensive scalings $E = O(N)$ and $M = O(N)$ as well as our system's variance conditions (2.13)- (2.15). We also assume finite dimensional Hilbert spaces for the subsystems. We define the diagonal average of any variable $X_{\alpha,m}$ as

$$\langle X_{\alpha,m}\rangle_{\text{diag}} = \sum_{\alpha,m} |C_{\alpha,m}|^2 X_{\alpha,m}. \tag{2.25}$$

We sum our variance conditions (2.14) and (2.15)

$$\langle \vec{S}^2\rangle - M^2 \leq O(N) \tag{2.26}$$

and evalulate the LHS with $|\psi(0)\rangle$:

$$\sum_{\alpha,m} |C_{\alpha,m}|^2 s_\alpha(s_\alpha+1) - M^2 \leq O(N). \tag{2.27}$$

The inequality is equivalent, by algebra and the normalization of $\{|C_{\alpha,m}|^2\}$, to

$$M + (2M+1)\sum_{\alpha,m} |C_{\alpha,m}|^2 (s_\alpha - M) + \sum_{\alpha,m} |C_{\alpha,m}|^2 (s_\alpha - M)^2 \leq O(N). \tag{2.28}$$

Since $M = \sum_{\alpha,m} |C_{\alpha,m}|^2 \, m$, we can replace the second term's $(s_\alpha - M)$ with $(s_\alpha - m)$. Recall that $m \leq s_\alpha$. Every factor on the inequality's LHS is therefore nonnegative, so every term must be $\leq O(N)$. Since $2M + 1 = O(N)$, the second term implies that $\sum_{\alpha,m} |C_{\alpha,m}|^2 (s_\alpha - M) \leq O(1)$. By the definition of $\langle . \rangle_{\text{diag}}$, we see

$$\langle s_\alpha\rangle_{\text{diag}} \leq M + O(1) \tag{2.29}$$

and from the third term in Eq. (2.28) we get the inequality

$$\langle (s_\alpha - M)^2 \rangle_{\text{diag}} \leq O(N) \tag{2.30}$$

by similar arguments.

We now upper-bound fairly general correlators' magnitudes. Let $x_1, x_2, \ldots, x_n$ denote real-valued functions of α and m. (For notational brevity, we suppress the functions' dependencies on α and m.) Let the functions' magnitudes obey the upper bound $|x_j| \leq X \in \mathbb{R} \ \ \forall j, \alpha, m$. We analyze correlator magnitudes of the form

$$\left| \langle x_1^{A_1} x_2^{A_2} \ldots x_n^{A_n} \rangle_{\text{diag}} \right| . \tag{2.31}$$

Without loss of generality, the powers are ordered from greatest to least: $A_1 \geq A_2 \geq \ldots \geq A_n \geq 0$. At-least-two-point correlators interest us, so $A \coloneqq \sum_{j=1}^{n} A_j \geq 2$. Therefore, either $A_1 \geq 2$ or $A_1 = A_2 = 1$. In the first case, we show, the correlator magnitude (2.31) is upper-bounded by X^{A-2} times $\langle x_1^2 \rangle$; in the second case, the correlator magnitude is upper-bounded by X^{A-2} times $\frac{1}{2} \langle x_1^2 + x_2^2 \rangle$. We parcel the factors so for reasons clarified below.

First, suppose that $A_1 \geq 2$. To upper-bound (2.31), we invoke the average's definition, then the triangle inequality:

$$\left| \langle x_1^{A_1} x_2^{A_2} \ldots x_n^{A_n} \rangle_{\text{diag}} \right| \leq \sum_{\alpha, m} |C_{\alpha,m}|^2 \, |x_1|^{A_1} |x_2|^{A_2} \cdots |x_n|^{A_n}. \tag{2.32}$$

We separate out a factor of $|x_1|^2$. Then, we bound the rest using the assumption $|x_j| \leq X$ and

the definition $A \coloneqq \sum_{j=1}^{n} A_j$:

$$\begin{aligned}\left|\langle x_1^{A_1} x_2^{A_2} \dots x_n^{A_n} \rangle_{\text{diag}}\right| &\leq \sum_{\alpha,m} |C_{\alpha,m}|^2 \, |x_1|^2 \cdot \underbrace{|x_1|^{A_1-2} |x_2|^{A_2} \cdots |x_n|^{A_n}}_{\leq X^{A-2}} \\ &\leq \langle x_1^2 \rangle_{\text{diag}} X^{A-2}. \end{aligned} \tag{2.33}$$

The final inequality follows from the reality of x_1.

Now, suppose that $A_1 = A_2 = 1$. To bound the correlator magnitude (2.31), we again invoke the average's definition, then the triangle inequality. This time, we separate $x_1^{A_1} x_2^{A_2} = x_1 x_2$ from the other variables:

$$\left|\langle x_1^{A_1} x_2^{A_2} \dots x_n^{A_n} \rangle_{\text{diag}}\right| \leq \sum_{\alpha,m} |C_{\alpha,m}|^2 \, |x_1 x_2| \cdot \underbrace{|x_3|^{A_3} |x_4|^{A_4} \cdots |x_n|^{A_n}}_{\leq X^{A-2}} . \tag{2.34}$$

Since x_1 and x_2 are real, $x_1^2 + x_2^2 - 2|x_1 x_2| = (|x_1| - |x_2|)^2 \geq 0$. Rearranging yields $|x_1 x_2| \leq \frac{1}{2}(x_1^2 + x_2^2)$. Combining this inequality with Ineq. (2.34), we obtain

$$\left|\langle x_1^{A_1} x_2^{A_2} \dots x_n^{A_n} \rangle_{\text{diag}}\right| \leq \frac{1}{2} \langle x_1^2 + x_2^2 \rangle_{\text{diag}} X^{A-2} . \tag{2.35}$$

Finally, we combine our previous results given by Eqs. (2.29), (2.30) and (2.35). Let (x_1, x_2, x_3) equal $(E_\alpha - E,\, m - M,\, s_\alpha - M)$. Since local subsystems have finite-dimensional Hilbert spaces, each variable is upper-bounded by some $O(N)$ number X. By the variance conditions, the functions $\langle x_j^2 \rangle_{\text{diag}}$ and $\frac{1}{2}\langle x_j^2 + x_k^2 \rangle_{\text{diag}}$ are $O(N)$ for all $j, k = 1, 2, 3$. Therefore, substituting into Eq. (2.33) yields the moment condition (2.24), as does substituting into Eq. (2.35).

We can now explain why we sought bounds that contained $\langle x_1^2 \rangle_{\text{diag}}$ or $\langle x_1^2 + x_2^2 \rangle_{\text{diag}}$. These averages are only $O(N)$. If we had treated x_1^2 or $x_1 x_2$ like the other variables, each would have

contributed an $O(N^2)$ factor to the corresponding bound. We would not have recovered the all-important -1 in the moment condition's exponent (2.24).

2.4.2 Clebsch-Gordan Coefficients for Extensive M

Having proven that both our ensembles have moment conditions that obey Eq. (2.24), we proceed to evaluate the thermal and quantum expectation value (2.23). Our probability distribution in both cases yield the moment conditions (2.24) and so each p_{α,m_α} is only large near $E_\alpha = E$, $m_\alpha = M$, and $s_\alpha = M$. The Clebsch-Gordan coefficients and $\mathcal{T}^{(k)}$ are smooth so we Taylor expand them about E and M. From our extensive quantities and z-axis-oriented system we have $s_\alpha \gg 1$ and $s_\alpha - m_\alpha \ll s_\alpha$. The general form of the Clebsch-Gordan coefficients is given by

$$\begin{aligned}
&\langle s_\alpha, m_\alpha | s_{\alpha'}, m_{\alpha'}; k, q\rangle = \delta_{m_\alpha, m_{\alpha'}+q} \\
&\times \sqrt{\frac{(2s_\alpha+1)\,(s_\alpha+s_{\alpha'}-k)!\,(s_\alpha-s_{\alpha'}+k)!\,(s_{\alpha'}+k-s_\alpha)!\,(s_\alpha+m_\alpha)!}{(s_\alpha+s_{\alpha'}+k+1)!}} \\
&\times \sqrt{(s_\alpha-m_\alpha)!\,(s_{\alpha'}-m_{\alpha'})!\,(s_{\alpha'}+m_{\alpha'})!\,(k-q)!\,(k+q)!} \\
&\times \sum_\ell \Bigg[\frac{(-1)^\ell}{\ell!\,(s_{\alpha'}+k-s_\alpha-\ell)!\,(s_{\alpha'}-m_{\alpha'}-\ell)!\,(k+q-\ell)}! \\
&\times \frac{1}{(s_\alpha-k+m_{\alpha'}+\ell)!\,(s_\alpha-s_{\alpha'}-q+\ell)!}\Bigg]
\end{aligned} \tag{2.36}$$

where the sum runs over all integer ℓ values for which every factorial's argument is nonnegative [29]. Setting $s_{\alpha'} = s_\alpha$, as was done in the time-averaged expectation value, and assuming

that $m_{\alpha'} > 0$ as prescribed by our system, we arrive at

$$\begin{aligned}\langle s_\alpha, m_\alpha | s_\alpha, m_{\alpha'}; k, q\rangle = \delta_{m_\alpha, m_{\alpha'}+q}\sqrt{\frac{(2s_\alpha+1)\,(2s_\alpha-k)!\,(k!)^2\,(s_\alpha+m_\alpha)!}{(2s_\alpha+k+1)!}} \\ \times \sqrt{(s_\alpha-m_\alpha)!\,(s_\alpha-m_{\alpha'})!\,(s_\alpha+m_{\alpha'})!\,(k-q)!\,(k+q)!} \\ \times \sum_\ell \Big[\frac{(-1)^\ell}{\ell!\,(k-\ell)!\,(s_\alpha-m_{\alpha'}-\ell)!} \\ \times \frac{1}{(k+q-\ell)!\,(s_\alpha-k+m_{\alpha'}+\ell)!\,(\ell-q)!}\Big]. \end{aligned} \tag{2.37}$$

The sum has the same condition on ℓ and the factorials imply six conditions on ℓ. Of the six, four are worth noting as two of them supersede two others since we take $q \geq 0$. The four constraints on ℓ are $\ell \leq k$, $\ell \leq s_\alpha - m_{\alpha'}$, $\ell \geq k - s_\alpha - m_{\alpha'}$ and $\ell \geq q$. These constraints can be summarized as

$$\ell \in \{q, q+1, ..., \min\{k, s_\alpha - m_{\alpha'}\}\}. \tag{2.38}$$

Continuing the simplification of the Clebsch-Gordan coefficients, we take $m_\alpha = m_{\alpha'} + q$ due to the Kronecker delta function and substitute the $O(1)$ variable $\Delta_{\alpha'} = s_\alpha - m_{\alpha'}$, giving

$$\begin{aligned}\langle s_\alpha, m_\alpha | s_\alpha, m_{\alpha'}; k, q\rangle = k!\sqrt{(\Delta_{\alpha'}-q)!\,\Delta_{\alpha'}!\,(k-q)!\,(k+q)!} \\ \times \sum_\ell \Big[\frac{(-1)^\ell}{\ell!\,(k-\ell)!\,(\Delta_{\alpha'}-\ell)!\,(k+q-\ell)!\,(\ell-q)!} \\ \times \sqrt{\frac{(2s_\alpha+1)(2s_\alpha-k)!(2s_\alpha-\Delta_{\alpha'}+q)!\,(2s_\alpha-\Delta_{\alpha'})!}{(2s_\alpha+k+1)!}} \\ \times \frac{1}{(2s_\alpha-\Delta_{\alpha'}-k+\ell)!}\Big]. \end{aligned} \tag{2.39}$$

Using Stirling's approximation for the extensive s_α factors and expanding the natural log function, the s_α-dependent factor becomes

$$(2s_\alpha)^{\frac{q}{2}-\ell}\exp(O(\frac{1}{s_\alpha})) = (2s_\alpha)^{\frac{q}{2}-\ell}(1+O(1/s_\alpha)) \tag{2.40}$$

where we can see the greatest contribution to our sum in Eq. (2.40) comes from the smallest ℓ value. By the constraints on ℓ, the least possible value is given by q. Replacing the sum in Eq. (2.40) with the $\ell = q$ term, switching from $m_{\alpha'}$ to m_α (for notational simplification only), and switching back from the $\Delta_{\alpha'}$, we get a form for the Clebsch-Gordan coefficients of

$$\frac{(-1)^q}{q!(2s_\alpha)^{q/2}}\left(\frac{(s_\alpha-m_\alpha)!\,(k+q)!}{(k-q)!\,(s_\alpha-m_\alpha-q)!}\right)[1+O\,(1/s_\alpha)] \tag{2.41}$$

or, written more intuitively,

$$\begin{aligned}\langle s_\alpha, m_\alpha+q|s_\alpha,m_\alpha;k,q\rangle = \frac{[-\mathrm{sgn}(q)]^q}{|q|!(2s_\alpha)^{|q|/2}}&\left(\frac{(s_\alpha-m_\alpha)!\,(k+|q|)!}{(s_\alpha-m_\alpha-|q|)!(k-|q|)!}\right)^{\frac{1}{2}}\\ &\times\left[1+O\left(\frac{1}{s_\alpha}\right)\right].\end{aligned} \tag{2.42}$$

With this in order, we turn our attention to the $\mathcal{T}^{(k)}$ function.

2.4.3 Approximation of the $\mathcal{T}^{(k)}$ Function

To see all corrections to thermal prediction we must also look at the scalings of the $\mathcal{T}^{(k)}$ function. While we usually write the $\mathcal{T}^{(k)}$ function as a function of energy, it is more generally a function of densities such as $\mathcal{E}/N$. This is because the $\mathcal{T}^{(k)}$ gives us single-site expectation values. Writing it as $\mathcal{T}^{(k)}\left(\frac{\mathcal{E}}{N},\frac{\mathcal{S}}{N}\right)$, we can approximate an order of magnitude for the derivatives as

$$\frac{\partial^a}{\partial\mathcal{E}^a}\frac{\partial^b}{\partial\mathcal{S}^b}\mathcal{T}^{(k)}(\mathcal{E},\mathcal{S}) = O\left(\frac{1}{N^{a+b}}\right). \tag{2.43}$$

As a result,

$$\mathcal{T}^{(k)}(E_\alpha, s_\alpha) = \mathcal{T}^k(E, M) + O\left(\frac{E_\alpha - E}{N}\right) + O\left(\frac{s_\alpha - M}{N}\right) + \dots \tag{2.44}$$

where the following terms are of order $([E_\alpha - E]^a[s_\alpha - M]^c]/N^{a+c})$. With this result we can finally retrieve deviations between thermal and quantum results.

2.4.4 Thermal and Quantum Result for $q = 0$

Expanding Eq. (2.42) when $q = 0$ and using our moment conditions (2.24) we can approximate the Clebsch-Gordon coefficients as

$$\langle s_\alpha, m_\alpha | s_\alpha, m_\alpha; k, 0\rangle = 1 + O\left(\frac{s_\alpha - M}{N}\right) + O\left(\frac{m_\alpha - M}{N}\right) + ... \tag{2.45}$$

where each following term is of order $([m_\alpha - M]^b[s_\alpha - M]^c]/N^{b+c})$. Plugging in our approximations for the Clebsch-Gordon coefficients and the $\mathcal{T}^{(k)}$ function we arrive at

$$\langle T_0^{(k)}\rangle_p = \sum_{\alpha, m_\alpha} p_{\alpha, m_\alpha}[\mathcal{T}^{(k)}(E, M) + O\left(\frac{E_\alpha - E}{N}\right) + O\left(\frac{s_\alpha - M}{N}\right) + O\left(\frac{m_\alpha - M}{N}\right) + ...]. \tag{2.46}$$

By the normalization constraint on the probabilities the first term can be taken out of the sum. By the moment conditions, the following terms are upper-bounded by $\leq O(N^{a+b+c-1}/N^{a+b+c}) = O\left(\frac{1}{N}\right)$. We therefore arrive at the conclusion that for an extensive M, and $q = 0$, both the thermal and quantum time-average for a $T_0^{(k)}$ operator is

$$\langle T_0^{(k)}\rangle_p = \mathcal{T}^{(k)}(E, M) + O\left(\frac{1}{N}\right) \tag{2.47}$$

hence suggesting that the thermal and quantum time averages are equal to each other within $O\left(\frac{1}{N}\right)$ corrections, as is the case with standard ETH.

2.4.5 Thermal and Quantum Result for $q \neq 0$

The thermal expectation value for $q \neq 0$ is simply 0. The time-averaged expectation value becomes a bit more unruly. The case of $q = 0$ allowed us to consider the diagonal ensemble probability distribution given by the $|C_{\alpha,m_\alpha}|^2$ and derive moment conditions. The comparison for $q \neq 0$ becomes more involved as the we no longer have a probability distribution in our quantum time-average (2.23) but instead a sum,

$$\overline{\langle T^{(k)}_{q\neq 0}\rangle_t} = \sum_{\alpha,m_\alpha} C^*_{\alpha,m_\alpha+q} C_{\alpha,m_\alpha} \langle s_\alpha, m_\alpha + q | s_\alpha, m_\alpha; k, q\rangle \mathcal{T}^{(k)}(E_\alpha, s_\alpha), \tag{2.48}$$

where we have $C^*_{\alpha,m_\alpha+q} C_{\alpha,m_\alpha}$. To circumvent this we make use of the Cauchy-Schwarz inequality to provide an upper bound on Eq. (2.48). Defining a vector $\vec{u}$ with components $u_{\alpha,m_\alpha} = C_{\alpha,m_\alpha+q}$, and a vector $\vec{v}$ with components $v_{\alpha,m_\alpha} = C_{\alpha,m_\alpha}\langle s_\alpha, m_\alpha + q | s_\alpha, m_\alpha; k, q\rangle$, the Cauchy-Schwarz inequality, which states $\vec{u}\cdot\vec{v} \leq \sqrt{\vec{u}\cdot\vec{u}}\sqrt{\vec{v}\cdot\vec{v}}$, yields

$$\begin{aligned}\overline{\langle T^{(k)}_{q\neq 0}\rangle_t} \leq & \sqrt{\sum_{\alpha,m_\alpha:|m_\alpha+q|\leq s_\alpha} |C_{\alpha,m_\alpha+q}|^2} \\ & \times \left\{ \sum_{\alpha',m_{\alpha'}} |C_{\alpha',m_{\alpha'}}|^2 \langle s_{\alpha',m_{\alpha'}+q} | s_{\alpha'}, m_{\alpha'}; k, q\rangle^2 [\mathcal{T}^{(k)}(E_\alpha, s_\alpha)]^2 \right\}^2 .\end{aligned} \tag{2.49}$$

This equation took advantage of the realness of the Clebsch-Gordon coefficients and $\mathcal{T}^{(k)}$. By the normalization condition on the C's we can upper bound the first sum by 1. In the same fashion as with the $q = 0$ case, the second sum is dominated by terms where $E_\alpha \sim E, m_\alpha \sim$

$M, s_\alpha \sim M$ and $s_\alpha - m_\alpha \ll s_\alpha$. Using Eq. (2.42) we can arrive at, for general q,

$$\langle s_\alpha, m_\alpha + q | s_\alpha, m_\alpha; k, q\rangle = O\left(\left[\frac{s_\alpha - m_\alpha}{2s_\alpha}\right]^{|q|/2}\right)\left[1 + O\left(\frac{1}{s_\alpha}\right)\right] \tag{2.50}$$

or

$$\langle s_\alpha, m_\alpha + q | s_\alpha, m_\alpha; k, q\rangle = O\left(N^{-|q|/2}\right)\left[1 + O\left(\frac{1}{s_\alpha}\right)\right]. \tag{2.51}$$

The reason for keeping the $O(1/s_\alpha)$ term in the brackets will prove to be necessary. First, consider the case $|q| \geq 2$. This gives a time-averaged expectation value of

$$\overline{\langle T^{(k)}_{|q|\geq 2}\rangle_t} \leq O\left(\frac{1}{N}\right). \tag{2.52}$$

The thermal and time-averaged expectation values may differ within $O\left(\frac{1}{N}\right)$ corrections, as typically expected. However, inserting $q = \pm 1$ into Eq. (2.51) may indeed make someone naïvely believe that there is a possible "anomalous thermalization" occurring as now the two expectation values may only differ by an $O(1/\sqrt{N})$ factor. This is not the case. In order to prove this we first look at the average of the standard raising operator, $\langle S_+\rangle$. We can write the average as $\langle S_+\rangle$ = $\langle S_x\rangle + i\langle S_y\rangle$ which is 0 by our system constraints. Using the fact that S_+ is a T^1_1 operator and how it acts on an eigenstate, we can write

$$\langle S_+\rangle = \sum_{\alpha, m_\alpha} C^*_{\alpha, m_\alpha + 1} C_{\alpha, m_\alpha} \sqrt{(s_\alpha - m_\alpha)(s_\alpha + m_\alpha + 1)} = 0. \tag{2.53}$$

Taylor approximating the large $\sqrt{s + m_a + 1}$ term as $\sqrt{2M+1}$ we see,

$$\begin{aligned}\langle S_+\rangle = \sqrt{2M+1} \sum_{\alpha, m_\alpha} & C^*_{\alpha, m_\alpha + 1} C_{\alpha, m_\alpha} \sqrt{(s_\alpha - m_\alpha)} \\ & \times \left[1 + O\left(\frac{s_\alpha - M}{N}\right) + O\left(\frac{m_\alpha - M}{N}\right)\right] = 0.\end{aligned} \tag{2.54}$$

For $q = \pm 1$ the Clebsch-Gordan coefficient (2.42) simplifies to

$$\langle s_\alpha, m_\alpha + 1 | s_\alpha, m_\alpha; k, q\rangle = -\text{sgn}(q)\sqrt{\frac{k(k+1)(s_\alpha - m_\alpha)}{2s_\alpha}}\left(1 + O\left(\frac{1}{s_\alpha}\right)\right). \tag{2.55}$$

Using this we can write

$$\begin{aligned}\overline{\langle T^{(k)}_{\pm 1}\rangle_t} = -\text{sgn}(q)\sqrt{\frac{k(k+1)}{2}}\sum_{\alpha, m_\alpha} C^*_{\alpha, m_\alpha + 1} C_{\alpha, m_\alpha}\sqrt{\frac{s_\alpha - m_\alpha}{s_\alpha}} \\ \times \left[1 + O\left(\frac{1}{s_\alpha}\right)\right]\mathcal{T}^{(k)}(E_\alpha, s_\alpha).\end{aligned} \tag{2.56}$$

Taylor expanding about our average values, $\frac{1}{\sqrt{s_\alpha}} = \frac{1}{\sqrt{M}}[1 + O(\frac{s_\alpha - M}{N})]$ and $\mathcal{T}^{(k)}(E_\alpha, s_\alpha) = \mathcal{T}^{(k)}(E, M) + O(\frac{E_\alpha - E}{N}) + O(\frac{1}{N})$, we arrive at

$$\begin{aligned}\overline{\langle T^{(k)}_{\pm 1}\rangle_t} = -\text{sgn}(q)\sqrt{\frac{k(k+1)}{2}}\frac{\mathcal{T}^{(k)}(E, M)}{\sqrt{M}}\sum_{\alpha, m_\alpha} C^*_{\alpha, m_\alpha + 1} C_{\alpha, m_\alpha}\sqrt{s_\alpha - m_\alpha} \\ \times \left[1 + O\left(\frac{s_\alpha - M}{N}\right) + O\left(\frac{E_\alpha - E}{N}\right) + O\left(\frac{1}{N}\right)\right].\end{aligned} \tag{2.57}$$

We see that the first term is exactly $\langle S_+\rangle$ to leading order; thus, to leading order, $\overline{\langle T^{(k)}_{\pm 1}\rangle_t} = 0$. Hence, the case for $q = \pm 1$ does not result in greater corrections than expected.

We have demonstrated that for a conserved extensive M, all k-local observables adhere to typical thermalization. In other words, no corrections were found which exceeded the expected $O(\frac{1}{N})$, in agreement with standard ETH.

2.5 Discussion and Conclusions

This work extended the eigenstate thermalization hypothesis to the general scenario of a system with non-commuting conserved charges. For our specific system and $O(N)$ observable

we retrieved thermal predictions from a quantum start point. This was possible by using an approximate microcanonical ensemble. An important mention is the possibility for *anomalous thermalization* where thermal and quantum results differ by an order greater than $O(N^{-1})$. In [19] we give a scenario where, for a different scaling of $M = 0$, one might expect anomalous thermalization by an $O(N^{-1/2})$ term. There are many different scenarios to explore for anomalous thermalization, such as $M = O(N^{\gamma})$ for $0 < \gamma < 1$. However, the possibility for anomalous thermalization is still up for discussion and is only mentioned for completeness.

While this analysis was system-specific, we expect it to hold for most systems with non-Abelian conserved charges, serving as a true extension of ETH.

Chapter 3

Microcanonical Truncations of Observables in Quantum Chaotic Systems

We consider the properties of an observable (such as a single spin component that squares to the identity) when expressed as a matrix in the basis of energy eigenstates, and then truncated to a microcanonical slice of energies of varying width. For a quantum chaotic system, we model the unitary or orthogonal matrix that relates the spin basis to the energy basis as a random matrix selected from the appropriate Haar measure. We find that the spectrum of eigenvalues is given by a centered Jacobi distribution that approaches the Wigner semicircle of a random hermitian matrix for small slices. We give a quantitative critical point for which the distribution *definitely* ceases to be semicircular. For slices that contain more than half the states, there is a set of eigenvalues of exactly ± 1. The transition to this qualitatively different behavior at half size is similar to that seen in other quantities such as entanglement entropy. Our results serve as a benchmark model for numerical calculations in realistic physical systems.

3.1 Introduction

The eigenstate thermalization hypothesis (ETH) [10, 12, 30, 13, 31, 32, 33] is now widely accepted as a microscopic mechanism that is able to explain how an isolated quantum many-body system can come to thermal equilibrium when starting from an initial pure state that appears to be far from equilibrium. ETH is expected to hold for a "chaotic" quantum system that is sufficiently far (in a parameter space of possible hamiltonians) from any point of integrability and which also does not exhibit many-body localization due to strong disorder. ETH then takes the form of an ansatz for the matrix elements (in the energy-eigenstate basis) of each observable A that would be measured in order to determine whether or not the system is in thermal equilibrium. This ansatz is

$$A_{ij} = \mathcal{A}(E)\delta_{ij} + e^{-S(E)/2} f(E,\omega) R_{ij}, \tag{3.1}$$

where $E = (E_i + E_j)/2$ is the average energy of the two eigenstates, $\omega = E_i - E_j$ is their energy difference, $S(E)$ is the thermodynamic entropy (logarithm of the density of states) at energy E, $\mathcal{A}(E)$ and $f(E,\omega)$ are smooth, real functions of their arguments, with $f(E,\omega) = f(E,-\omega)$, and R_{ij} varies erratically, with overall zero mean and unit variance in local ranges of E and ω.

A question of interest is whether more can be said about the statistical properties of the R_{ij}'s. An argument based on the central limit theorem would indicate that they can be treated as independent gaussian random variables, and numerical investigations in specific systems have generally been consistent with this. However, as has been pointed out before [34, 35], this gaussianity cannot be an exact property, as it would yield various unphysical predictions, including an expression of any n-point time correlation function of A in terms of the 2-point function. Furthermore, the operator A has a spectrum of eigenvalues, and this spectrum must somehow be encoded in the energy-basis matrix elements A_{ij}. Because of this, as noted in

[34], it is more useful to think of the unitary matrix U_{ai} that transforms basis states in which A is diagonal to the energy-eigenstate basis as a statistically random matrix.

In [35] (see also [36]), the observable A was taken to be a component of a single spin in a lattice spin system, and the eigenvalues of A_{ij} computed when i and j were restricted to particular ranges of energies. If this submatrix had the statistical properties of a gaussian random matrix, then a Wigner semi-circular distribution of eigenvalues would be expected. This was found for small energy ranges, but significant deviations appeared at larger ranges.

Our goal here is to provide a theoretical benchmark for these calculations, computing the expected eigenvalue spectrum for a single-spin-component operator A (which obeys $A^2 = I$) when its matrix A_{ij} in the energy-eigenstate basis is truncated, with the energies E_i and E_j each in the same finite range. We refer to this as a microcanonical slicing. We specialize to the case where the $\mathcal{A}(E)$ function in Eq. (3.1) is zero; this is equivalent to

$$\mathrm{Tr} e^{-\beta H} A = 0 \tag{3.2}$$

for all inverse temperatures β. This corresponds to a system in which the hamiltonian H is invariant under $A \to -A$. We then treat the diagonalizing matrix U as either a unitary or orthogonal Haar-random matrix. (The result is the same in both cases.) This is the strongest possible assumption of random-matrix behavior; for an actual physical system, we expect correlations that result in U having an approximately banded structure. We hope that our benchmark results can be used in the future to help elucidate this structure in different physical systems of interest.

3.2 Microcanonical Truncations of an Observable Operator

We consider an operator A that obeys $A^2 = I$ and $\mathrm{Tr} A = 0$. We take the dimension of the full Hilbert space to be $2D$; for a system of N two-component spins, we would have $2D = 2^N$.

The eigenvalues of A are hence ± 1, with D eigenvalues of each sign.

We then write

$$A = U^\dagger \tilde{A} U, \tag{3.3}$$

where $\tilde{A}$ is a $2D \times 2D$ diagonal matrix,

$$\tilde{A} = \begin{pmatrix} +I & 0 \\ 0 & -I \end{pmatrix}, \tag{3.4}$$

and U is a unitary (or orthogonal) matrix that transforms from the computational basis (in which a component of each spin is diagonal) to the energy basis (in which the hamiltonian is diagonal).

We are now interested in a microcanonical slicing of A, defined as

$$A_K = \Pi_K A \Pi_K \tag{3.5}$$

where Π_K is a projection operator onto an energy window that spans K energy eigenstates.

We first specialize to the case $K \leq D$. We treat U as either a unitary or orthogonal matrix that is selected at random from the corresponding Haar measure, and consider the expected distribution $\rho(\lambda)$ of the eigenvalues λ of A_K in the limit of large D.

This problem has been solved in the context of products of random projectors[1] [37], and the result (for either unitary or orthogonal U) is a special case of the centered Jacobi distribution,

$$\rho(\lambda) = \frac{\sqrt{4\alpha(1-\alpha) - \lambda^2}}{2\pi\alpha(1-\lambda^2)}, \tag{3.6}$$

[1] These products have the form $\Pi_k \Pi \Pi_k$, which our problem can be mapped to by making the substitution $\Pi = \frac{1}{2}(A + I)$.

where we have defined

$$\alpha = \frac{K}{2D}, \tag{3.7}$$

and where $\rho(\lambda)$ vanishes for values of λ for which the argument of the square-root is negative. We have normalized $\rho(\lambda)$ to integrate to one.

For a thin microcanonical slice, $K \ll D$ and hence $\alpha \ll 1$, the maximum value of λ^2 is $4\alpha \ll 1$, and then we can replace $1 - \lambda^2$ in the denominator of Eq. (3.6) with 1. We then have

$$\rho_{\alpha \ll 1}(\lambda) \simeq \frac{1}{2\pi\alpha}\sqrt{4\alpha - \lambda^2}. \tag{3.8}$$

We can compare this result with the Wigner semicircle for an $K \times K$ hermitian random matrix H with matrix elements H_{ij} drawn from a gaussian distribution with the expected value of $|H_{ij}|^2$, $i \neq j$, given by v^2; this is [38]

$$\rho_{\mathrm{W}}(\lambda) = \frac{1}{2\pi K v^2}\sqrt{4Kv^2 - \lambda^2}. \tag{3.9}$$

Our $2D \times 2D$ matrix A obeys $A^2 = I$, and hence

$$\sum_{j=1}^{2D} |A_{ij}|^2 = 1. \tag{3.10}$$

This implies that the expected value of each $|A_{ij}|^2$ is $1/2D$. If we set $v^2 = 1/2D$ in Eq. (3.9), we find that Eq. (3.8) matches it. This result agrees with the expectation from ETH that, for small energy differences, the energy-basis matrix elements of a local observable should have the statistics of independent gaussian random variables.

For larger values of α, Eq. (3.6) begins to differ from the Wigner semicircle. The curvature at the origin $\rho''(0)$ is one diagnostic; it is negative for $\alpha < \alpha_{\mathrm{c}} = (2 - \sqrt{2})/4 = 0.146$ but turns positive for $\alpha > \alpha_{\mathrm{c}}$. This can be thought of as a critical point where the distribution definitely

ceases to be a Wigner semicircle. At $\alpha = 1/2$, $K = D$, we find an arcsine distribution with integrable singularities at $\lambda = \pm 1$,

$$\rho_{\alpha=1/2}(\lambda) = \frac{1}{\pi\sqrt{1-\lambda^2}}. \tag{3.11}$$

In Fig. 3.1(a,b,c), we show the eigenvalue distribution for a matrix with $2D = 10,000$ and with U a particular orthogonal matrix selected at random from the Haar measure, and with $K/2D = \alpha = 1/8, 1/4, 1/2$, along with the predicted distribution of Eq. (3.6). We find very good agreement.

Next we consider the case $K \geq D$. This can be related to the case $K \leq D$ by considering the complementary microcanonical projection operator,

$$\mathit{\Pi}_{2D-K} = I - \mathit{\Pi}_K. \tag{3.12}$$

For $K > D$ the eigenvalues of A_K are minus those of A_{2D-K}, plus $K - D$ extra pairs of eigenvalues of exactly ± 1. This is true for any specific individual U. To see this We write $A = U^\dagger \tilde{A} U$ in block-diagonal form,

$$A = \begin{pmatrix} A_K & B \\ B^\dagger & A_{2D-K} \end{pmatrix}. \tag{3.13}$$

We take $K \leq 2D$. Since the eigenvalues of A are ± 1, we have

$$A^2 = I. \tag{3.14}$$

This yields the three equations

$$A_K^2 + BB^\dagger = I, \tag{3.15}$$

$$A_K B + B A_{2D-K} = 0, \tag{3.16}$$

$$B^\dagger B + A_{2D-K}^2 = I. \tag{3.17}$$

We can make independent unitary transformations on the upper $K \times K$ block and on the lower $(2D-K) \times (2D-K)$ block that render A_K and A_{2D-K} diagonal. We then write

$$(A_K)_{ij} = \lambda_i \delta_{ij}, \quad (A_{2D-K})_{i'j'} = \kappa_{i'} \delta_{i'j'}, \tag{3.18}$$

where $i, j = 1, \ldots, K$ and $i', j' = K+1, \ldots, 2D-K$. Taking the ij' matrix element of Eq. (3.16), we get

$$(\lambda_i + \kappa_{j'}) B_{ij'} = 0. \tag{3.19}$$

This shows that a nonvanishing matrix element of B is possible if and only if there is an eigenvalue $\kappa_{j'}$ of A_{2D-K} that is the negative of an eigenvalue λ_i of A_K. For $K < D$, there are more eigenvalues of A_{2D-K} than there are of A_K, and Eq. (3.17) then implies that these extra eigenvalues must be ± 1. Since $\mathrm{Tr} A = 0$, these extra eigenvalues must come in ± 1 pairs.

We conclude that, for $K \leq D$, the $2D-K$ eigenvalues of A_{2D-K} consist of K eigenvalues that are equal in magnitude and opposite in sign to the K eigenvalues of A_K, $D-K$ eigenvalues $+1$, and $D-K$ eigenvalues -1.

Hence, after averaging U over a Haar measure, the result will be a continuous spectrum given by Eq. (3.6) (though with the normalizing factor of α in the denominator replaced by $1-\alpha$), plus a discrete spectrum of $K-D$ eigenvalues $+1$ and $K-D$ eigenvalues -1.

In Fig. 3.1(d,e), we show the eigenvalue distribution for $K/2D = \alpha = 3/4, 7/8$. We find, as predicted, a continuous distribution that matches that of the matrix with $K/2D = 1-\alpha$,

with all remaining eigenvalues exactly equal to ± 1.

These results for $K > D$ are contrary to our initial expectations. We expected to find the Wigner semicircle for $K \ll D$, and for this to gradually morph into a set of only ± 1 at $K = 2D$. Our expectations are met by the results for $K \leq D$, but the sudden appearance of some exact ± 1 eigenvalues for every $K > D$, along with an additional continuous distribution that mirrors the distribution for $K < D$ and eventually becomes a Wigner semicircle for small $2D - K$, came as a surprise to us. We will discuss this further in our conclusions.

3.3 Conclusions

Motivated by the investigations of [35], we have considered the properties of a single spin-component operator (with eigenvalues that are an equal number of plus ones and minus ones) in a many-body quantum-chaotic system. We are interested in the statistical properties of the matrix elements of such an operator in the energy-eigenstate basis. We model this by treating the unitary (or orthogonal) matrix U that relates the spin-eigenstate basis to the energy-eigenstate basis as a random matrix selected from the Haar measure. We then consider microcanonical truncations of this matrix in the energy basis, and study their eigenvalues. For truncations to a much smaller matrix, we find the distribution agrees with the Wigner semicircle expected for a hermitian random matrix. For larger truncations, we find that the truncated matrix begins to "remember" that the eigenvalues of the full matrix are ± 1.

Once the truncation is to a matrix larger than half the size of the original, we find that there are now a set of eigenvalues of exactly ± 1, along with a continuous distribution that matches that of the complementary truncation. This result was counter to what we initially expected, and shows a kind of phase transition at half system size. This is reminiscent of a similar transition in the behavior of entanglement and Rényi entropies [39], which also exhibit sudden changes of behavior at half system size. Similar transitions have also been discussed in

[40] for operators that include more than half the degrees of freedom of the system.

Our results are based on the most chaotic possible behavior of a physical system, in which the energy eigenstates are completely random superpositions of basis states, without any additional structure. Though this is unlikely to be true for any realistic physical system, our results serve as a useful benchmark of comparison for numerical calculations in these systems.

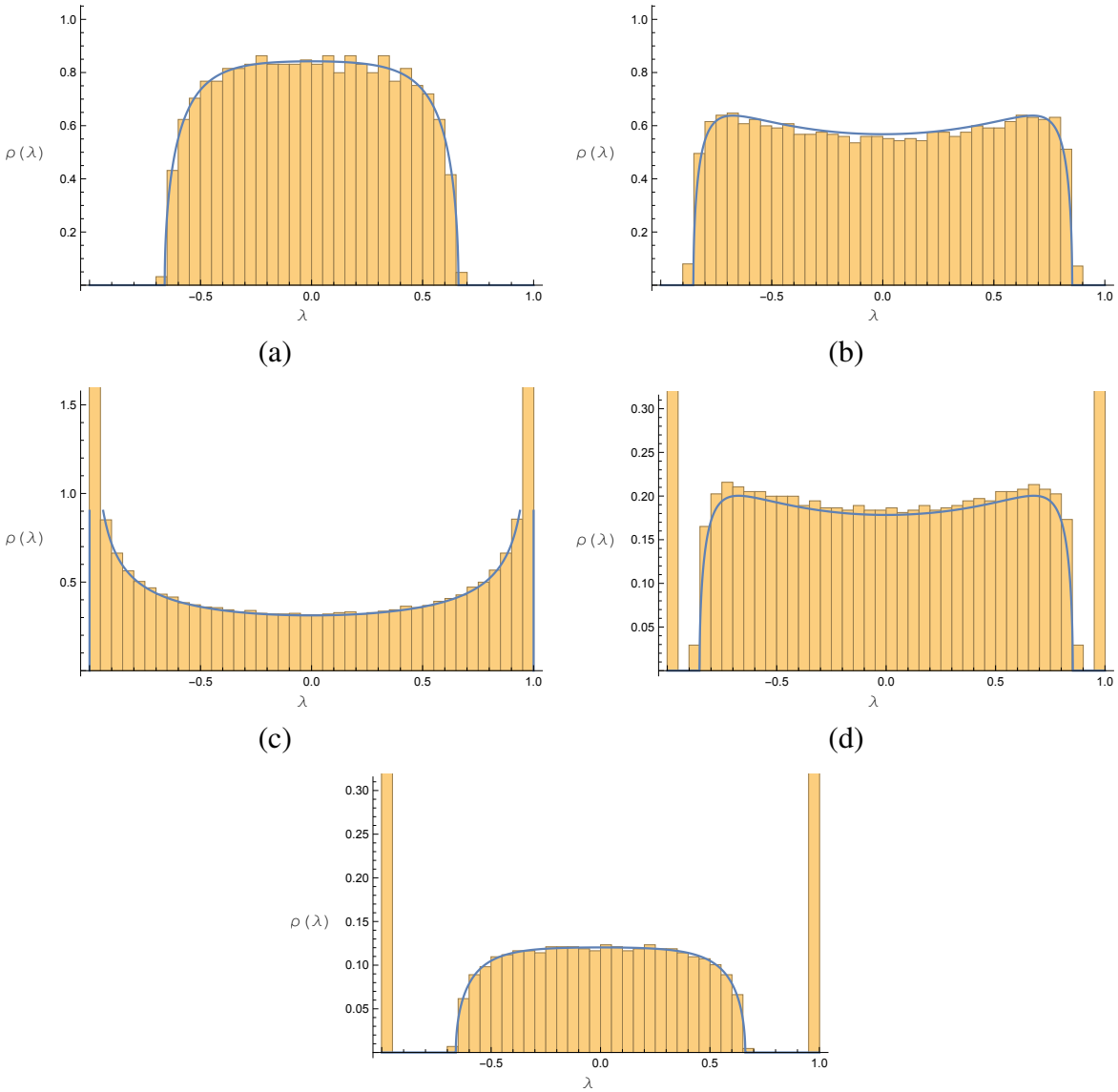

Figure 3.1: Histograms of eigenvalues for different microcanonical truncation sizes of an originally 10000×10000 matrix ($2D = 10000$). The blue curve represents the analytical prediction given by the Jacobi distribution of Eq. (3.6). Figs. (a)–(e) show results for $K/2D = 0.125, 0.25, 0.5, 0.75, 0.875$. Figs. (d) and (e) are truncated in height and do not show the full count of ± 1 eigenvalues.

Chapter 4

Quantum Fisher Information for Different States and Processes in Quantum Chaotic Systems

In this chapter, we discuss the ability to distinguish between an energy eigenstate that obeys ETH and a truly thermal density matrix. The quantum Fisher information (QFI) associated with a particular process applied to a many-body quantum system has been suggested as a diagnostic for the nature of the system's quantum state, e.g., a thermal density matrix vs. a pure state in a system that obeys the eigenstate thermalization hypothesis (ETH). We compute the QFI for both an energy eigenstate and a thermal density matrix for a variety of processes in a system obeying ETH, including a change in the hamiltonian that is either sudden (a quench), slow (adiabatic), or followed by contact with a heat bath.

4.1 Introduction

Quantum Fisher information (QFI; for an introduction and review, see [41]) has recently received renewed attention as a diagnostic tool for understanding properties of quantum many-body systems [42, 43]. The QFI for a one-parameter family of density operators ρ_θ is designated F_θ, and one of its key properties is that it sets the minimum uncertainty $\Delta\theta$ in the value of θ after an ideal measurement. Specifically, for a single ideal measurement, the Cramér–Rao bound is

$$(\Delta\theta)^2 \geq \frac{1}{F_\theta}. \tag{4.1}$$

This can be viewed as a generalized form of the uncertainty principle.

In practice, we are most interested in density operators ρ_θ whose θ dependence is due to some specific experimental manipulation on a base ρ_0, such as a local unitary transformation of the form $\rho_\theta = U_\theta^\dagger \rho_0 U_\theta$ with $U_\theta = \exp(-i\theta A)$ for some local hermitian operator A. This corresponds to an experimental set-up in which the experimenter has direct control of the physical quantity represented by A, such as a single qubit.

In [42], the QFI for a system whose quantum state is a thermal density matrix that is subjected to this type of local unitary transformation was expressed in terms of a particular dynamical susceptibility. In [43], it was pointed out that, in a system that obeys the eigenstate thermalization hypothesis (ETH), the QFI for an energy eigenstate differs from the the QFI for a thermal density matrix when both are subjected to the same local unitary transformation. This makes the QFI a useful theoretical tool for distinguishing pure and mixed states that are not distinguished by measurements of local observables. In this regard the QFI is comparable to the von Neumann entropy and Rényi entropies of ρ_θ.

In this work, in addition to the local unitary transformation described above, we consider three other possible experimental protocols performed on a quantum chaotic system: an adiabatic transformation, in which the system's hamiltonian is very slowly changed; a quench, in

which the system's hamiltonian is suddenly changed and the system is then allowed to evolve in time under the new hamiltonian (this case has been discussed previously in [44]); and a rethermalization, in which a system that was initially thermalized by contact with a heat bath has its hamiltonian changed, and then is put back in contact with the same heat bath. We compute the QFI for these transformations for an energy eigenstate and for a thermal density matrix (only the latter in the case of rethermalization).

4.2 Quantum Fisher Information

The QFI is given formally by

$$F_\theta = \mathrm{Tr} L_\theta^2 \rho_\theta, \tag{4.2}$$

where L_θ (the symmetric logarithmic derivative) is an operator that is defined implicitly via

$$\rho'_\theta = \tfrac{1}{2}\big(L_\theta \rho_\theta + \rho_\theta L_\theta\big), \tag{4.3}$$

where the prime denotes a derivative with respect to θ. Eq. (4.1) holds if the rank of ρ_θ does not change as θ is varied over a small range around its base value [45], which will always be the case in this work.

A more explicit formula for the QFI follows from the spectral decomposition of ρ_θ,

$$\rho_\theta = \sum_i p_i |i\rangle\langle i|, \tag{4.4}$$

where the states $\{|i\rangle\}$ form an orthonormal and complete basis, and the probabilities p_i obey $0 \leq p_i \leq 1$ and $\sum_i p_i = 1$. (These states and probabilities depend on θ, but we do not denote

this explicitly.) We then have

$$F_\theta = 2 \sum_{ij}{}' \frac{|\langle i|\rho'_\theta|j\rangle|^2}{p_i + p_j}, \tag{4.5}$$

where the prime on the sum means that terms for which $p_i + p_j = 0$ (if any) are omitted.

Because of the linearity of quantum mechanics, in all cases of practical interest ρ'_θ is linearly related to ρ_θ. For the four specific types of transformations that we consider, this linear relation takes the form

$$\rho'_\theta = i[B, \rho_\theta] + D\rho_\theta, \tag{4.6}$$

where B and D are hermitian operators with $[D, \rho_\theta] = 0$ and $\mathrm{Tr}D\rho_\theta = 0$. We note that the normalization condition $\mathrm{Tr}\rho_\theta = 1$ implies $\mathrm{Tr}\rho'_\theta = 0$, which is satisfied by Eq. (4.6). Using Eq. (4.6) in Eq. (4.5), we get

$$F_\theta = 2 \sum_{ij}{}' \frac{(p_i - p_j)^2}{p_i + p_j} |\langle i|B|j\rangle|^2 + \sum_i p_i |\langle i|D|i\rangle|^2. \tag{4.7}$$

For a transformation that is unitary (which is the case for all but one of the transformations we consider), we have $D = 0$. In this case, an important relation obeyed by F_θ is

$$F_\theta \leq 4(\Delta B)^2, \tag{4.8}$$

where

$$(\Delta B)^2 = \mathrm{Tr}\rho_\theta B^2 - (\mathrm{Tr}\rho_\theta B)^2 \tag{4.9}$$

is the quantum variance in the expectation value of B in the state ρ_θ. Eq. (4.8) becomes an equality if and only if ρ_θ is a pure state. Thus the QFI of a mixed state is strictly less than that of a pure state with the same quantum variance of B.

Note that Eqs. (4.1,4.8,4.9) yield $(\Delta\theta)(\Delta B) \geq 1/2$, which is a more recognizable form of the uncertainty principle.

4.3 Experimental protocols

We consider four types of experimental protocols that transform an initial reference state ρ_0 to ρ_θ.

Local unitary. We set

$$\rho_\theta = e^{i\theta A}\rho_0 e^{-i\theta A}, \tag{4.10}$$

where A is a dimensionless local hermitian operator. This is the form of ρ_θ that is treated in [43].

Adiabatic. The hamiltonian is slowly changed from H to

$$H_\theta = H + \theta\mu A, \tag{4.11}$$

where μ is a constant with dimensions of energy. (This constant could be absorbed into either θ or A, but we prefer to keep both these quantities dimensionless to facilitate comparison of different transformation protocols.) As H is slowly changed from H to H_θ, an eigenstate $|\alpha\rangle$ of H evolves adiabatically to an eigenstate $|\alpha\rangle_\theta$ of H_θ. Hence, an initial density operator ρ_0 evolves to

$$\rho_\theta = \sum_{\alpha,\beta} |\alpha\rangle_\theta\langle\alpha|\rho_0|\beta\rangle\langle\beta|_\theta. \tag{4.12}$$

This is a unitary transformation.

Quench. The hamiltonian is suddenly changed from H to H_θ, Eq. (4.11), and the system then evolves unitarily under H_θ for a time t. This yields

$$\rho_\theta = e^{-iH_\theta t}\rho_< e^{iH_\theta t}, \tag{4.13}$$

where $\rho_<$ is the state of the system just before the quench at $t = 0$. This differs from ρ_0, which is defined as the state of the system with $\theta = 0$ at time t. In terms of ρ_0, Eq. (4.13) becomes

$$\rho_\theta = e^{-iH_\theta t} e^{iHt} \rho_0 e^{-iHt} e^{iH_\theta t}. \tag{4.14}$$

This is a unitary transformation.

Rethermalization. For this protocol, we specialize to the case that the initial state is a thermal density operator for the hamiltonian H at an inverse temperature β,

$$\rho_0 = Z_0^{-1} e^{-\beta H}, \tag{4.15}$$

where $Z_0 = \mathrm{Tr} e^{-\beta H}$. The density operator ρ_θ is then taken to be a thermal density operator at the same inverse temperature β, but now with hamiltonian H_θ, Eq. (4.11),

$$\rho_\theta = Z_\theta^{-1} e^{-\beta H_\theta}, \tag{4.16}$$

where $Z_\theta = \mathrm{Tr} e^{-\beta H_\theta}$. This protocol corresponds to putting the system (with hamiltonian H) in contact with a heat bath at inverse temperature β, then changing the hamiltonian to H_θ, and then putting the system back into contact with the same heat bath. This is not a unitary transformation.

We now compute ρ_0' for each of these transformations (for an arbitrary ρ_0) and identify the operators B and D in Eq. (4.6), which then yields the QFI via Eq. (4.7).

For any unitary transformation (which includes our local unitary, adiabatic, and quench transformations), we have

$$D = 0 \quad \text{(local unitary, adiabatic, quench)}. \tag{4.17}$$

For the local unitary transformation of Eq. (4.10), taking the derivative with respect to θ and comparing to Eq. (4.6) yields

$$B = A \quad \text{(local unitary)}. \tag{4.18}$$

For the adiabatic transformation of Eq. (4.11), an eigenstate $|\alpha\rangle_\theta$ of H_θ is found from Rayleigh-Schrodinger perturbation theory to be

$$|\alpha\rangle_\theta = |\alpha\rangle + \theta\mu \sum_\gamma{}' \frac{A_{\gamma\alpha}}{E_\alpha - E_\gamma}|\gamma\rangle + O(\theta^2), \tag{4.19}$$

where the prime means that $\gamma = \alpha$ is omitted, and $|\alpha\rangle$ is an eigenstate of H with eigenvalue E_α,

$$H|\alpha\rangle = E_\alpha|\alpha\rangle. \tag{4.20}$$

Using Eq. (4.19) in Eq. (4.12) and taking the derivative with respect to θ, we get Eq. (4.6) with the matrix elements of B (in the energy eigenstate basis) given by

$$B_{\alpha\beta} = \begin{cases} 0 & \text{if } \alpha = \beta \\ \dfrac{i\mu A_{\alpha\beta}}{E_\alpha - E_\beta} & \text{if } \alpha \neq \beta \end{cases} \quad \text{(adiabatic)}. \tag{4.21}$$

We note that these matrix elements of B are the same as the matrix elements of the adiabatic gauge potential, a quantity introduced in [46] as a diagnostic tool for quantum chaos.

The quench transformation of Eq. (4.14) is unitary, and we can express B via

$$B = -i\frac{\partial}{\partial\theta} e^{-iH_\theta t} e^{iHt}\Big|_{\theta=0} \tag{4.22}$$

We start with the general identity [47]

$$\frac{\partial}{\partial\theta}e^{-iH_\theta t} = -i\int_0^t dt' e^{-iH_\theta t'}\left(\frac{\partial H_\theta}{\partial\theta}\right)e^{-iH_\theta(t-t')}. \tag{4.23}$$

Setting $H_\theta = H + \theta\mu A$ and using Eq. (4.23) in Eq. (4.22), we get

$$B = -\int_0^t dt' e^{-iHt'}\mu A e^{iHt'} \tag{4.24}$$

for the case of a quench. Sandwiching Eq. (4.24) between two different energy eigenstates $\langle\alpha|$ and $|\beta\rangle$, and performing the integral over t', we obtain the off-diagonal matrix elements

$$B_{\alpha\beta} = \frac{1-e^{-i(E_\alpha-E_\beta)}t}{E_\alpha - E_\beta}i\mu A_{\alpha\beta}. \tag{4.25}$$

Taking the limit $E_\beta \to E_\alpha$ yields the diagonal matrix elements

$$B_{\alpha\alpha} = -\mu t A_{\alpha\alpha}. \tag{4.26}$$

Hence the matrix elements are

$$B_{\alpha\beta} = \begin{cases} -\mu t A_{\alpha\alpha} & \text{if } \alpha = \beta \\ \dfrac{1-e^{-i(E_\alpha-E_\beta)t}}{E_\alpha - E_\beta}i\mu A_{\alpha\beta} & \text{if } \alpha \neq \beta \end{cases} \quad \text{(quench)}. \tag{4.27}$$

For the rethermalization transformation of Eq. (4.16), once again we begin by taking the derivative with respect to θ of ρ_θ as given by Eq. (4.16),

$$\frac{\partial}{\partial\theta}\rho_\theta = \frac{1}{Z_\theta}\frac{\partial}{\partial\theta}e^{-\beta H_\theta} - \frac{1}{Z_\theta^2}\frac{\partial Z_\theta}{\partial\theta}e^{-\beta H_\theta}. \tag{4.28}$$

Applying Eq. (4.23) with $t \to -i\beta$ and $t' \to -i\beta'$ and setting $\theta = 0$ yields

$$\rho_0' = -\frac{1}{Z_0}\int_0^\beta d\beta' e^{-\beta' H}\mu A e^{-(\beta-\beta')H} + \frac{1}{Z_0^2}e^{-\beta H}\mathrm{Tr}\int_0^\beta d\beta' e^{-\beta' H}\mu A e^{-(\beta-\beta')H}. \tag{4.29}$$

Using the cyclic property of the trace in the second term, we get

$$\rho_0' = -\frac{1}{Z_0}\int_0^\beta d\beta' e^{-\beta' H}\mu A e^{-(\beta-\beta')H} + \beta\mu\langle A\rangle\rho_0, \tag{4.30}$$

where $\langle A\rangle = \mathrm{Tr}\rho_0 A$.

Sandwiching Eq. (4.30) between two different energy eigenstates $\langle\alpha|$ and $|\beta\rangle$ yields zero from the second term since ρ_0 is diagonal in the energy basis. Performing the integral over β' in the first term then results in the off-diagonal matrix elements

$$\langle\alpha|\rho_0'|\beta\rangle = \frac{1}{Z_0}\big(e^{-\beta E_\alpha} - e^{-\beta E_\beta}\big)\frac{\mu A_{\alpha\beta}}{E_\alpha - E_\beta}. \tag{4.31}$$

Using $\rho_0 = Z_0^{-1}e^{-\beta H}$, we have

$$\langle\alpha|[B,\rho_0]|\beta\rangle = -\frac{1}{Z_0}\big(e^{-\beta E_\alpha} - e^{-\beta E_\beta}\big)B_{\alpha\beta}. \tag{4.32}$$

Using Eq. (4.6) and comparing with Eq. (4.31), we identify the off-diagonal matrix elements of B as those of Eq. (4.35).

The diagonal elements of B can be set to zero, since they do not appear in Eq. (4.7) for any ρ_0 that is diagonal in the energy basis, which is the only case we consider for rethermalization.

Sandwiching Eq. (4.30) between identical energy eigenstates $\langle\alpha|$ and $|\alpha\rangle$ yields the limit of Eq. (4.31) as $E_\beta \to E_\alpha$, plus the expectation value of the second term on the right-hand side of Eq. (4.30),

$$\langle\alpha|\rho_0'|\alpha\rangle = -\frac{1}{Z_0}e^{-\beta E_\alpha}\beta\mu\big(A_{\alpha\alpha} - \langle A\rangle\big). \tag{4.33}$$

We also have, using $[D, \rho_0] = 0$,

$$\langle\alpha|D\rho_0|\alpha\rangle = \frac{1}{Z_0} e^{-\beta E_\alpha} D_{\alpha\alpha}. \tag{4.34}$$

Our results take the form

$$B_{\alpha\beta} = \begin{cases} 0 & \text{if } \alpha = \beta \\ \dfrac{i\mu A_{\alpha\beta}}{E_\alpha - E_\beta} & \text{if } \alpha \neq \beta \end{cases} \quad \text{(rethermalization)} \tag{4.35}$$

and

$$D_{\alpha\alpha} = -\beta\mu\big(A_{\alpha\alpha} - \langle A\rangle\big) \quad \text{(rethermalization)}, \tag{4.36}$$

where

$$\langle A\rangle = \mathrm{Tr}\rho_0 A. \tag{4.37}$$

In addition to specifying the experimental protocols, we must also specify the initial state. As in [43], we compare and contrast the results for an initial energy eigenstate and a thermal density operator with the same energy. Our results can be straightforwardly generalized to other classes of initial states, both pure and mixed; we comment briefly on this in the conclusions.

We also note that for any ρ_0 that is diagonal in the energy basis, the diagonal elements $B_{\alpha\alpha}$ of B drop out of the right-hand side of Eq. (4.6), and hence do not affect the value of the QFI.

4.4 An Even Briefer Review of ETH

We assume that the system of interest is a closed, finite, chaotic many-body system (with $N \gg 1$ degrees of freedom). Our working definition of *chaotic* is that each few-body observable A obeys ETH, which states that the matrix elements of A in the energy basis take the

form [13]

$$A_{\alpha\beta} = \mathcal{A}(E)\delta_{\alpha\beta} + e^{-S(E)/2} f(E,\omega) R_{\alpha\beta}, \tag{4.38}$$

where $E = (E_\alpha + E_\beta)/2$ is the average energy of the two eigenstates, $\omega = E_\alpha - E_\beta$ is the energy difference, $S(E)$ is the thermodynamic entropy (logarithm of the density of states) at energy E, $\mathcal{A}(E)$ and $f(E,\omega)$ are smooth, real functions of their arguments, with $f(E,\omega) = f(E,-\omega)$, and $R_{\alpha\beta}$ is a hermitian matrix of erratically varying elements, with overall zero mean and unit variance in local ranges of E and ω. The function $f(E,\omega)$ can be related to the dynamical susceptibility of A [43]. We take E to be an extensive quantity ($E \sim N$) and ω to be an intensive quantity ($\omega \sim 1$). In accord with this, we assume that the initial state ρ_0 yields an expectation value of the energy that is extensive,

$$E = \mathrm{Tr}\rho_0 H \sim N, \tag{4.39}$$

and a quantum energy uncertainty that is sub-extensive,

$$\Delta E = [\mathrm{Tr}\rho_0 (H-E)^2]^{1/2} \sim N^\nu, \quad \nu < 1. \tag{4.40}$$

We note that for a thermal state, $\nu = 1/2$.

4.5 Computing QFI

We begin by considering an initial energy eigenstate, $\rho_0 = |\alpha\rangle\langle\alpha|$, and a local unitary transformation, Eq. (4.10), which yields Eq. (4.18). Since the initial state is pure, Eq. (4.8) holds as an equality. Using Eq. (4.9) and inserting a complete set of energy eigenstates, we have

$$F_0 = 4\sum_{\beta\neq\alpha} |A_{\alpha\beta}|^2. \quad \text{(local unitary)}. \tag{4.41}$$

We now use the ETH ansatz of Eq. (4.38). We replace $|R_{\alpha\beta}|^2$ by its statistical average of 1 over a small range of E_β, and convert the sum over β to an integral over E_β; this integral includes a density-of-states factor of $\exp S(E_\beta)$. We then change the integration variable to $\omega = E_\alpha - E_\beta$. The result is

$$F_0 = 4 \int_{-\infty}^{+\infty} d\omega \, e^{S(E_\alpha - \omega) - S(E_\alpha - \omega/2)} |f(E_\alpha + \omega/2, \omega)|^2. \tag{4.42}$$

Treating E_α as extensive and ω as intensive, we can Taylor expand the $S(E)$ factors using $\beta := S'(E_\alpha)$, where β is the inverse temperature of the system when the energy is E_α. We can also neglect the shift of E_α in the first argument of $f(E, \omega)$. Finally, we can use the fact that $f(E, \omega)$ is an even function of ω. The result is

$$F_0 = 4 \int_{-\infty}^{+\infty} d\omega \cosh\Big(\frac{\beta\omega}{2}\Big) |f(E, \omega)|^2. \quad \text{(local unitary)}, \tag{4.43}$$

is in agreement with [43]. We have dropped the α index on E for notational simplicity. At small ω, we generally expect $f(E, \omega)$ to approach a nonzero constant, and at large ω, $|f(E, \omega)|^2$ goes to zero faster than $\exp(-\beta|\omega|/2)$ [48]. Hence this integral converges.

For the other two transformation protocols that we consider in the case of an initial energy eigenstate (adiabatic and quench), we express our results in terms of a function $K(\omega)$, defined via

$$F_0 = 4 \int_{-\infty}^{+\infty} d\omega \, K(\omega) \, \cosh\Big(\frac{\beta\omega}{2}\Big) |f(E, \omega)|^2. \tag{4.44}$$

As we have already seen, for an energy eigenstate (es) and a local unitary transformation (lu), we have

$$K_{\text{es,lu}}(\omega) = 1. \tag{4.45}$$

For an initial energy eigenstate and adiabatic transformation (ad), we can deduce $K(\omega)$ by

comparing Eq. (4.21) with Eq. (4.18). We see that

$$K_{\mathrm{es,ad}}(\omega) = \frac{\mu^2}{\omega^2}. \tag{4.46}$$

Since we generically expect $f(E,\omega)$ to approach a nonzero constant as $\omega \to 0$, the integral in Eq. (4.44) diverges at low ω. There is a lower cutoff at the mean level spacing $\Delta \sim \exp[-S(E)]$, so in this case the QFI is exponentially large, $F_0 \sim \exp S(E)$. Note, however, that for the transformation to be truly adiabatic, with negligible possibility of changing energy levels, it must be done over an equally exponentially large time.

For a quench (qu), we get $K(\omega)$ by comparing Eq. (4.27) with Eq. (4.18). We find

$$K_{\mathrm{es,qu}}(\omega) = 4\frac{\mu^2}{\omega^2}\sin^2\Big(\frac{\omega t}{2}\Big). \tag{4.47}$$

In this case, $K_{\mathrm{es,qu}}(\omega) \to \mu^2 t^2$ as $\omega \to 0$, and so the integral in Eq. (4.44) does not diverge at low ω. In the limit of large t, following the standard procedure used to derive Fermi's Golden Rule for a transition rate, we can make the replacement

$$\frac{1}{\omega^2}\sin^2\Big(\frac{\omega t}{2}\Big) \to \frac{\pi}{2}|t|\delta(\omega). \tag{4.48}$$

This implies that at late times after the quench, the QFI grows at a constant rate of

$$\frac{dF_0}{dt} = 8\pi\mu^2|f(E,0)|^2. \tag{4.49}$$

After an exponentially long time, due to the discreteness of the energy levels, this will saturate at the exponentially large value $F_0 \sim \exp S(E)$ that we found for an equally long adiabatic transformation.

We now consider a thermal initial state, Eq. (4.15). This is diagonal in the energy basis,

with $p_\alpha = e^{-\beta E_\alpha}/Z_0$. Hence Eq. (4.7) becomes

$$F_0 = 2 \sum_{\alpha,\beta}{}' \frac{(p_\alpha - p_\beta)^2}{p_\alpha + p_\beta} |B_{\alpha\beta}|^2. \tag{4.50}$$

For a local unitary transformation we have $B = A$. We use the ETH ansatz of Eq. (4.38), replace $|R_{\alpha\beta}|^2$ by its average of 1 over small energy ranges, and convert the sums to integrals over E_α and E_β, including a density-of-states factor of $\exp S$ for each. We then change the integration variables to $E = (E_\alpha + E_\beta)/2$, $\omega = E_\alpha - E_\beta$. The result is

$$F_0 = \frac{4}{Z_0} \int_{E,\omega} e^{S(E) - \beta E} \frac{\sinh^2(\beta\omega/2)}{\cosh(\beta\omega/2)} |f(E,\omega)|^2, \tag{4.51}$$

where $\int_{E,\omega} \coloneqq \int_0^\infty dE \int_{-\infty}^{+\infty} d\omega$. Performing the integral over E by Laplace's method fixes the value of E at the solution of $S'(E) = \beta$, and yields a factor of Z_0. Hence for a thermal initial state and a local unitary transformation, we get Eq. (4.44) with

$$K_{\mathrm{th,lu}}(\omega) = \tanh^2\Big(\frac{\beta\omega}{2}\Big), \tag{4.52}$$

The integral in Eq. (4.44) then converges at both high and low ω. This result is in agreement with [43].

The relative factor between $K_{\mathrm{es,lu}}$ and $K_{\mathrm{th,lu}}$ comes solely from the different spectrum of p_α, and hence the same relation holds for the other transformations,

$$K_{\mathrm{th},i}(\omega) = \tanh^2\Big(\frac{\beta\omega}{2}\Big) K_{\mathrm{es},i}(\omega), \tag{4.53}$$

where $i = \mathrm{lu}, \mathrm{ad}, \mathrm{qu}$. Hence for a thermal initial state and an adiabatic transformation, we have

$$K_{\mathrm{th,ad}}(\omega) = \frac{\mu^2}{\omega^2} \tanh^2\Big(\frac{\beta\omega}{2}\Big). \tag{4.54}$$

For a a thermal initial state and a quench, we have

$$K_{\mathrm{th,qu}}(\omega) = 4\frac{\mu^2}{\omega^2}\tanh^2\Big(\frac{\beta\omega}{2}\Big)\sin^2\Big(\frac{\omega t}{2}\Big). \tag{4.55}$$

For the adiabatic and quench transformations, the integral in Eq. (4.44) converges at both high and low ω. For the quench in the limit of large t, we can make the replacement

$$\sin^2\Big(\frac{\omega t}{2}\Big) \to \frac{1}{2} \tag{4.56}$$

instead of Eq. (4.48); the difference is due to the differing behavior of the integrand at low ω. The QFI in the case of a quench then approaches a constant value, equal to twice its value in the adiabatic case.

For rethermalization, a comparison of Eq. (4.35) with Eq. (4.18) yields

$$K_{\mathrm{th,re}}(\omega) = \frac{\mu^2}{\omega^2}\tanh^2\Big(\frac{\beta\omega}{2}\Big), \tag{4.57}$$

which is the same as the adiabatic case for a thermal initial state.

4.6 Conclusions

We have computed the QFI for several different possible experimental protocols performed on a quantum many-body system that obeys ETH. The results are expressed in terms of a form-factor $K(\omega)$ via Eq. (4.44). The difference between an energy eigenstate and a thermal density matrix is the same for all protocols, and is given by Eq. (4.53), in agreement with the results of [43].

The most dramatic difference occurs for an adiabatic transformation, where the QFI is exponentially larger for a thermal density matrix than for an energy eigenstate (but the trans-

formation must be made exponentially slowly). After a quench, the QFI grows linearly with time for a thermal density matrix while it remains constant for an energy eigenstate.

The results for an energy eigenstate will also hold for "typical" pure state with a non-extensive energy uncertainty. By "typical", we mean a state whose expansion coefficients in the energy-eigenstate basis are uncorrelated with the matrix elements of the transformation operator A.

For a similarly "typical" mixed state, the results will depend on the details of the spectrum of probabilities p_i in the diagonalizing basis.

We have thus seen that the QFI is a valuable theoretical diagnostic tool. Its value distinguishes between a self-thermalized pure state in a quantum-chaotic system and a true thermal density matrix, and furthermore distinguishes among different experimental measurement protocols, allowing for a precise characterization of the measurement uncertainty in these different situations.

Chapter 5

Entanglement Negativity Transitions in Chaotic Eigenstates

In this chapter, we derive corrections to the leading order term in entanglement negativity in chaotic eigenstates. Entanglement negativity is an entanglement measure defined on a bipartite density matrix that is feasibly computable. We focus on a particular transition previously studied in a toy model of JT gravity, one for which the sum over permutations was found to give similar (or even stronger) enhanced corrections compared to entanglement entropy. Using a simplification, we derive and resum the relevant permutations to give a form for the averaged negativity spectrum, reproducing the gravitational answer for some quantities and finding tension with other quantities, namely the partially transposed entropy.

5.1 Introduction

Bipartite entanglement has been a heavily studied subject as it has implications for many areas of research. While entanglement entropy has become a staple of quantum mechanics, it is not generalizable to determine if true quantum entanglement is present in mixed quantum

states [49]. For a pure quantum state, the entanglement entropy is zero if it is not entangled and non-zero otherwise. Determining if a generic state is entangled is an NP-hard problem [50]. There is no quantity known which is zero if a mixed state is quantum untangled and non-zero otherwise. Another point of interest is determining entanglement in a multipartite system, where entanglement entropy also fails to do. A diagnostic tool for quantum entanglement in bipartite or tripartite (at most) systems that has gained a lot of traction in recent years is entanglement negativity.

First introduced in [51], entanglement negativity is a feasibly computable measure of entanglement when compared to other candidates such as entanglement cost [52]. Entanglement negativity has been used to characterized mixed state entanglement in free bosonic and fermionic systems [53, 54, 55, 56, 57], one-dimensional conformal field theory [58, 59, 60], spin chains [61, 62], and topologically ordered phases [63, 64]. Furthermore, it has been used as a diagnostic for quantum thermalization [65], information recovery in evaporating black holes [66], and other holographic contexts [67].

Recently, it was shown by [67] that similar enhanced corrections to the leading order term, such as the ones discussed in [68, 69, 70] for the entanglement entropy, exist near transitions in entanglement negativity used as a tripartite entanglement measure defined on a bipartite density matrix $\rho_{A_1A_2}$. In particular, the logarithmic negativity was shown to have the following form at transition:

$$\mathcal{E}(\rho_{R_1R_2}) = \log k_2 - \frac{\pi^2}{8\beta} + \mathcal{O}(\log \beta), \tag{5.1}$$

for two subsystems R_1 and R_2 with $R_1 \cup R_2 = R$. Further corrections were derived for measures descending from a Rényi version of negativity.

There exists a rich phase diagram for entanglement negativity in holographic states, and we show that a similar phase diagram exists for a generic chaotic eigenstate for the specific model considered here. Our aim is to systematically derive the corrections at transitions in this

phase space. There are two possible transitions, but as was explored in [67] we only expect interesting behavior near one of the transitions, for reasons that will be recapitulated shortly.

5.2 Entanglement Negativity

In this section we compute similar quantities as [70] for entanglement negativity measures. We begin by reviewing some salient properties of entanglement negativity and its utility as a tripartite measure of entanglement before diving into the calculation.

5.2.1 Review of Negativity

Entanglement negativity refers to an entanglement measure based on properties of the partial transpose operation applied to a bipartite density matrix $\rho_{A_1A_2}$, defined via

$$\langle a_1, a_2|\rho_{A_1A_2}^{T_{A_2}}|a_1', a_2'\rangle = \langle a_1, a_2'|\rho_{A_1A_2}|a_1', a_2\rangle \tag{5.2}$$

for basis states $\{|a_1\rangle\}$ in A_1 and $\{|a_2\rangle\}$ in A_2 [51, 71, 72]. The partial transpose is a positive but not completely positive map, which means some of the eigenvalues of $\rho_{A_1A_2}^{T_{A_2}}$ (hereafter $\rho_{A_1A_2}^{T_2}$) can be negative. Entanglement negativity quantifies the different between the eigenvalues of the partially transposed density matrix and the original density matrix via

$$\mathcal{N}(\rho_{A_1A_2}) = \sum_i \frac{|\lambda_i| - \lambda_i}{2} = \sum_{i:\lambda_i<0} |\lambda_i|. \tag{5.3}$$

In other words, the entanglement negativity is a measure of how much the partially transposed density matrix fails to be positive definite. Since the entanglement negativity depends only on the trace norm of the partially transposed density matrix it is feasibly computable. Any state that has a density matrix that is separable has a partially transposed density matrix which is

also separable with $\mathcal{N} = 0$ [73]. However, states with $\mathcal{N} = 0$ may still be entangled. Some further properties of entanglement negativity: it is convex, it does not increase under mixing, it is not additive, and it is an entanglement monotone (does not increase under local operations and classical communications (LOCC)). Entanglement negativity provides a lower bound on how close a state can be taken to a specific mixed state by means of LOCC, a lower bound on teleportation distance, and an upper-bound on teleportation results.

As with the von Neumann entropy, there exist Rényi generalizations of entanglement negativity:

$$\mathcal{N}_n = \mathrm{Tr}\left(\rho_{A_1A_2}^{T_2}\right)^n. \tag{5.4}$$

Due to the absolute value, one needs to define two different analytic continuations for even and odd Rényi index n, so there are in fact two Rényi negativities given by

$$\begin{aligned}\mathcal{N}_{2k}^{(\text{even})} &= \sum_i |\lambda_i|^{2k} \\ \mathcal{N}_{2k-1}^{(\text{odd})} &= \sum_i \mathrm{sgn}(\lambda_i)|\lambda_i|^{2k-1}\end{aligned} \tag{5.5}$$

for integer k. We define relevant entanglement measures via analytic continuation from these quantities. The most common quantity to talk about is the logarithmic negativity, given via a $k \to 1/2$ analytic continuation of the even Rényi negativity

$$\mathcal{E}(\rho_{A_1A_2}) = \lim_{k\to 1/2} \log \mathcal{N}_{2k}^{(\text{even})}(\rho_{A_1A_2}) = \log \sum_i |\lambda_i|. \tag{5.6}$$

The most important use of the logarithmic negativity is that it upper bounds the entanglement of distillation of the bipartite system [51].

One other quantity of interest is the partially transposed entropy, also known as the odd entropy, which is related to the $k \to 1$ analytic continuation of the odd Rényi negativity and is

explicitly given by

$$S^{T_2} \equiv \lim_{k\to 1} \frac{1}{2k-2} \log \mathcal{N}_{2k-1} = -\sum_i \lambda_i \log|\lambda_i|. \tag{5.7}$$

We need to include the Rényi entropy-like singular term out front as $\mathcal{N}_1^{(\text{odd})} = \text{Tr}\rho_{A_1A_2}^{T_2} = 1$.

5.2.2 Ensemble Averaged Negativity

We can now discuss the ensemble average of the Rényi negativity in the gaussian approximation. The Schmidt decomposition of a generic energy eigenstate $|E\rangle$ defined on a tripartite system can be written as

$$|E\rangle = \sum_{i_1 j_1 J} M_{ijJ} |E_i\rangle_{A_1} \otimes |E_j\rangle_{A_2} \otimes |E_J\rangle_B \tag{5.8}$$

where the subscripts denote eigenstates of the subsystem hamiltonians H_{A_1}, H_{A_2} and H_B, respectively. As is convention, we use lowercase indices for states of A and uppercase indices for states of B. The eigenstate thermalization hypothesis (ETH) instructs us to think of M_{ijJ} as a gaussian random variable with zero mean and energy banded with width Δ [74, 39]. In particular, for a system with spatial dimension $d \geq 2$, we have the ansatz

$$M_{ijJ} = e^{-S(E_{A_i}+E_{A_j}+E_{B_J})/2} \left(\frac{e^{-\epsilon^2/2\Delta^2}}{\sqrt{2\pi}\Delta}\right)^{1/2} C_{ijJ}, \tag{5.9}$$

where $\epsilon = E_{A_i} + E_{A_j} + E_{B_J} - E$ is the deviation from the total microcanonical energy. When averaged over a small energy band in E_{A_i}, E_{A_j} and E_B, the random coefficients C_{ijJ} satisfy

$$\overline{C_{ijJ}} = 0, \quad \overline{C_{ijJ}C_{i'j'J'}} = \delta_{ii'}\delta_{jj'}\delta_{JJ'}. \tag{5.10}$$

The effects of finite Δ will not affect the current and future computation, so we work in the limit $\Delta \to 0$, where we approximate

$$M_{ijJ} \approx e^{-S(E)/2} C_{ijJ}. \tag{5.11}$$

The partially transposed density matrix is

$$\rho_{A_1A_2}^{T_2} = \frac{1}{\mathcal{N}} \sum_{E_i E_j E_J} C_{i_1 j_1 J} C_{i_2 j_2 J} |E_{i_1}, E_{j_2}\rangle\langle E_{i_2}, E_{j_1}|, \tag{5.12}$$

or, by replacing dummy variables

$$\rho_{A_1A_2}^{T_2} = \frac{1}{\mathcal{N}} \sum_{E_i E_j E_J} C_{i_1 j_2 J} C_{i_2 j_1 J} |E_{i_1}, E_{j_1}\rangle\langle E_{i_2}, E_{j_2}|, \tag{5.13}$$

where the sum over energies is understood to be in a window of width 3Δ, though again we take this width to vanish. We also have

$$\left(\rho_{A_1A_2}^{T_2}\right)^n = \frac{1}{\mathcal{N}^n} \sum_{E_{i_1}, E_{j_1}} \sum_{i_1,\cdots,i_n,j_1,\cdots,j_n,J_1,\cdots J_n} \prod_{m=1}^{n} C_{i_m j_{m+1} J_m} C_{i_{m+1} j_m J_m} |E_{i_1}, E_{j_1}\rangle\langle E_{i_{n+1}}, E_{j_{n+1}}|. \tag{5.14}$$

Note that the partial transpose has made it so the i (A_1) indices are contracted cyclically, while the j (A_2) indices are contracted anti-cyclically. The resolvent equation for these Wick contractions is the same as derived in [67] and we briefly cover the general idea.

A resolvent exists for the ensemble averaging over Wick contractions for the partially transposed density matrix $\rho_{A_1A_2}^{T_2}$. We work in the regime where $S_{A_2} \ll S_{A_1} + S_B$. The resolvent equation is [67]

$$\lambda R(\lambda)_{j_1 j_2}^{i_1 i_2} = \delta_{j_1 j_2}^{i_1 i_2} + e^{S_B} \left(\sum_{m=1}^{\infty} \frac{R(\lambda)^{2m-2}}{e^{(2m-2)S_{A_2}}} R(\lambda)_{j_1 j_2}^{i_1 i_2} + \sum_{m=1}^{\infty} \frac{R(\lambda)^{2m-1}}{e^{(2m-2)S_{A_2}}} R(\lambda)_{j_1 j_2}^{i_1 i_2} \right) \tag{5.15}$$

Taking the trace:

$$\lambda R(\lambda) = e^{S_{A_1}+S_{A_2}} + e^{S_B}\left(\sum_{m=1}^{\infty} \frac{R(\lambda)^{2m-1}(1+R(\lambda))}{e^{(2m-2)S_{A_2}}}\right) \tag{5.16}$$

and resumming gives the final resolvent equation

$$\lambda R(\lambda) = e^{S_{A_1}+S_{A_2}} + \frac{e^{S_B}}{e^{S_{A_2}}}\frac{R(\lambda)(1+R(\lambda))}{1-e^{2S_{A_2}}R(\lambda)^2}. \tag{5.17}$$

We recognize this as the resolvent equation for the moments of a block transposed Wishart matrix. In the case $S_{A_2} = 0$ this reduces to the resolvent equation for the untransposed density matrix. This is a cubic equation and can be solved exactly, but the solution is not enlightening.

In the case of entanglement entropy, it is seen that the moments of a Wishart matrix are given in closed form by a sum of Narayana numbers [70]. This is derived by an inverse Stieltjes transform of the appropriate resolvent and a generating function for the Narayana numbers gives the eigenvalue spectrum of a Wishart matrix. The inverse Stieltjes transform of the solution to Eq. (5.17), a generating function for the moments of a block transposed Wishart matrix ("block transposed Narayana numbers"), will produce the eigenvalue spectrum of a block transposed Wishart matrix (the "negativity spectrum"). The block transposed Narayana numbers are not known in closed form; see [75] for a recursive definition.

This resolvent equation furnishes a negativity spectrum described by the phase diagram in Figure 5.1. There are two transitions to consider. The first is when the A and B subsystems are the same size, i.e. $S_{A_1} + S_{A_2} = S_B$, corresponding to the transition from $g = \mathbb{1}$ to $g = \tau$ in the phase diagram. From the calculation in [67], we don't expect any enhanced corrections at this transition, so we don't study it in any detail, though the calculation would presumably follow the same steps. The second transition of interest is when the A_1 subsystem is the same size as the combined A_2B subsystem, $S_{A_1} = S_{A_2} + S_B$, corresponding to the transition from $g = \tau$ to

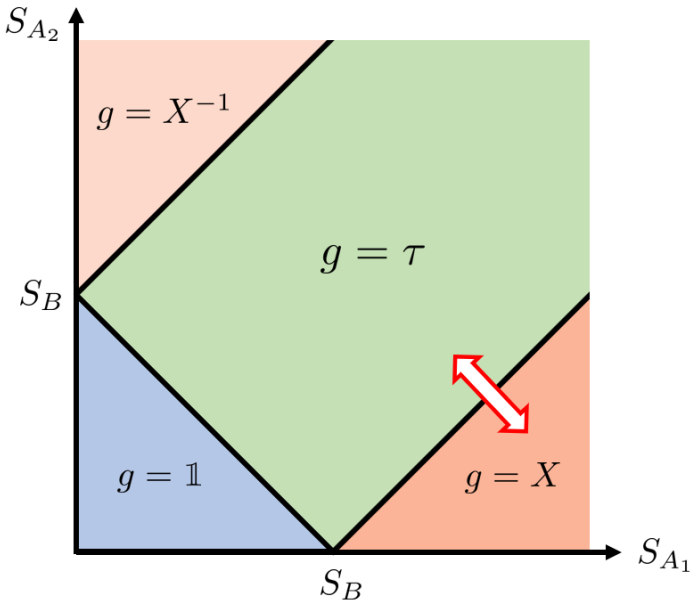

Figure 5.1: Phase diagram of Rényi negativity for various subsystem densities of state. The g's label the dominant permutation which appears in the sum over Wick contractions. The resolvent equation (5.17) is valid in the regime $S_{A_2} << S_{A_1} + S_B$; we've indicated the forbidden region $g = X^{-1}$ in a lighter shade. Reproduced with minor alterations from [67].

$g = X$ in the phase diagram.

Let's recall a few facts about the permutation group. For an element $g \in S_n$, we denote the number of swaps from the identity permutation $\mathbb{1} = (1)(2)\cdots(n)$ to g by $\ell(g)$ and the number of distinct cycles in g by $\chi(g)$. These quantities satisfy the relation

$$\ell(g) + \chi(g) = n \tag{5.18}$$

The number of swaps between two permutations $\ell(g^{-1}h) \equiv d(g,h)$ introduces a natural distance measure between two permutations. In particular, there exists the traingle inequality

$$d(g,g_1) + d(g_1,h) \geq d(g,h) \tag{5.19}$$

A *geodesic* between two permutations $G(g,h)$ is the set of $g_1's$ which saturate this inequality.

The sum over permutations we're interested in takes the form [76, 67, 66]

$$\texttt{SUM} = \sum_{g \in S_n} (e^{S_B})^m (e^{S_{A_1}})^p (e^{S_{A_2}})^q \tag{5.20}$$

where we've made the substitutions

$$m = \chi(g), \quad p = \chi(g^{-1}X), \quad q = \chi(g^{-1}X^{-1}) \tag{5.21}$$

Here X is the cyclic permutation $(12\cdots n)$ and X^{-1} is the anti-cyclic permutation $(n\ n-1\cdots 1)$. This is the sum relevant for calculating the moments of a block transposed Wishart matrix [75], i.e. the weighting of Wick contractions when averaging over a random density matrix with gaussian correlations. In our work, we're interested in the permutations which live on the geodesic $G(\mathbb{1}, X)$ and the geodesic $G(X, X^{-1})$ but not necessarily on the geodesic $G(\mathbb{1}, X^{-1})$. These permutations satisfy the following three equations:

$$\begin{aligned} m + p &= n + 1 \\ m + q &\leq n + 1 \\ p + q &= n + f(n) \end{aligned} \tag{5.22}$$

where the function $f(n) = 1$ if n is odd and 2 if n is even. When the second inequality is saturated, we're talking about the set of non-crossing pairings τ. There are C_n of these permutations, where C_n are the Catalan numbers

$$C_n = \frac{1}{n+1}\binom{2n}{n} \tag{5.23}$$

An example of a τ permutation on an even number of elements is $(12)(34)\cdots(n-1\ n)$. A non-crossing pairing on an odd number of elements will have a single cycle of length 1 and all other

cycles of length 2. Permutations which live on $G(\mathbb{1}, X)$ and $G(X, X^{-1})$ but not $G(\mathbb{1}, X^{-1})$ are precisely those which live on the single geodesic $G(\tau, X)$, which is the phase transition we're interested in. How do we enumerate these permutations? From the two equalities, we have:

$$p = n - 1 - mq = m + f(n) - 1 \tag{5.24}$$

From this, we can derive an upper bound on m:

$$m \leq \frac{n + 2 - f(n)}{2} \tag{5.25}$$

So we've reduced the sum over all permutations to a sum over a single parameter $m = \chi(g)$. We now have

$$\texttt{SUM} = \sum_{m=1}^{\frac{n-f(n)+2}{2}} T'(n,m) \left(e^{S_{A_2}}\right)^{f(n)-1} \left(e^{S_{A_1}}\right)^{n+1} \left(\frac{e^{S_B} e^{S_{A_2}}}{e^{S_{A_1}}}\right)^m \tag{5.26}$$

for some counting function $T'(n, m)$ which denotes the multiplicity at every $\chi(g)$. What is this function? Let's consider it for both even and odd n. For even $n = 2k$, the sum is

$$\texttt{EVEN SUM} = \sum_{m=1}^{k} T_e(k,m) e^{S_{A_2}} \left(e^{S_{A_1}}\right)^{2k+1} \left(\frac{e^{S_B} e^{S_{A_2}}}{e^{S_{A_1}}}\right)^m \tag{5.27}$$

This is a sum over permutations starting with the cyclic permutation X at $m = 1$ and ending with the pairwise connected permutations τ at $m = k$. Each m corresponds to a permutation with m cycles of even length. In this case, the numbers $T_e(k, m)$ are equivalent to the number of 2-Dyck paths of order k with m peaks and are given by

$$T_e(k,m) = \frac{1}{k} \binom{k}{m} \binom{2k}{m-1} \tag{5.28}$$

The $T_e(k,m)$ that appear here are analogous to the Narayana numbers which appear in the sum over non-crossing permutations. They are sometimes referred to as 2-Narayana numbers and appeared in various contexts elsewhere [77, 78, 79]. We therefore have

$$\begin{aligned}\texttt{EVEN SUM} &= e^{S_{A_2}}\left(e^{S_{A_1}}\right)^{2k+1}\sum_{m=1}^{k}T_e(k,m)\left(\frac{e^{S_B}e^{S_{A_2}}}{e^{S_{A_1}}}\right)^m \\ &= e^{2kS_{A_1}}e^{2S_{A_2}}e^{S_B}{}_2F_1\left(1-k,-2k,2;\frac{e^{S_B}e^{S_{A_2}}}{e^{S_{A_1}}}\right)\end{aligned} \tag{5.29}$$

Now let's look at the odd case. When $n = 2k-1$, the sum over permutations is

$$\texttt{ODD SUM} = \sum_{m=1}^{k}T_o(k,m)\left(e^{S_{A_1}}\right)^{2k}\left(\frac{e^{S_B}e^{S_{A_2}}}{e^{S_{A_1}}}\right)^m \tag{5.30}$$

Now the counting function is slightly different. We can derive it as follows: consider a permutation allowed in the even sum (5.27) with m cycles. The second binomial factor in Eq. (5.28) can morally be thought of as choosing $m-1$ distinct elements to belong to different cycles, while the rest is a symmetry factor that controls the number of non-crossing permutations modulo that choice. Therefore, one can think of each non-crossing permutation as living in a "labelled" superselection sector of size $\binom{2k}{m-1}$. By ignoring this choice and dividing by this factor, we can find a degenerate set of "unlabelled" non-crossing permutations. From this set we can remove an element from each cycle, so one unlabelled permutation in the even sum generates m distinct unlabelled permutations in the odd sum, which then have to be relabelled to give the correct counting. This strategy of unlabelling, removing an element, and relabelling gives us

$$T_o(k,m) = m\frac{\binom{2k-1}{m-1}}{\binom{2k}{m-1}}T_e(k,m) = \binom{2k-1}{m-1}\binom{k-1}{m-1} \tag{5.31}$$

If that was a bit too abstract, we illustrate this procedure in Figure 5.2. The sum over permuta-

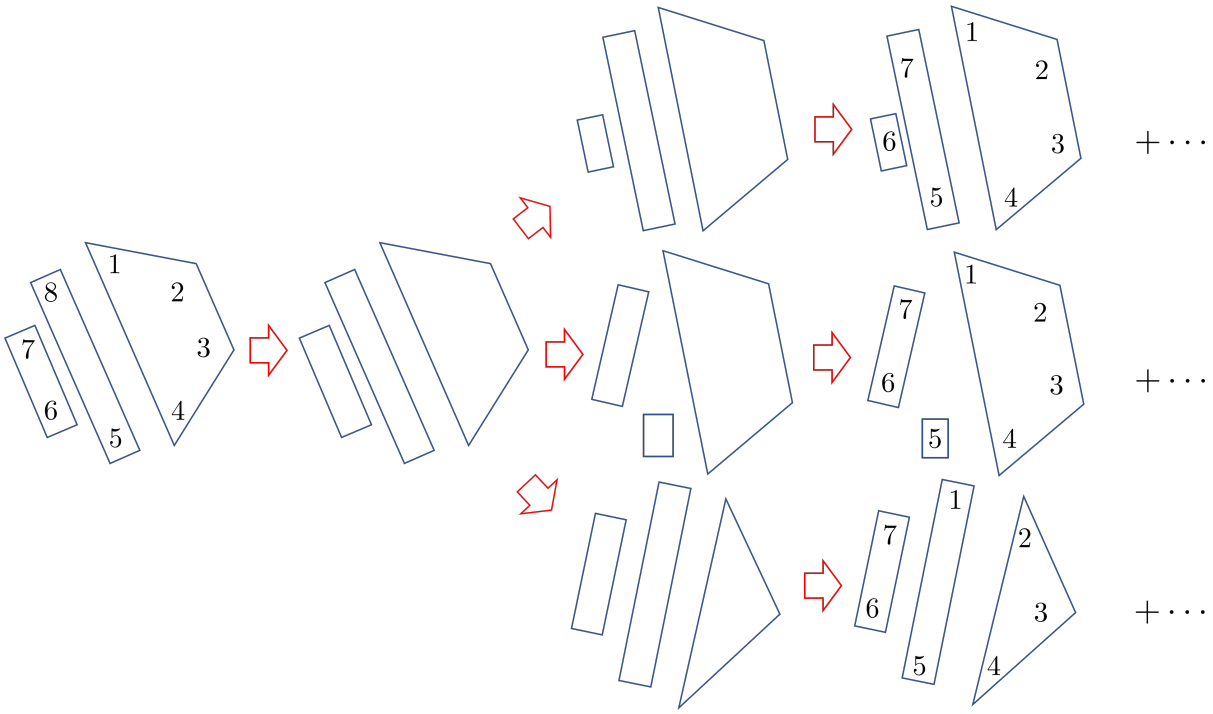

Figure 5.2: The procedure of generating permutations on $G(\tau, X)$ for odd n from even n. We identify even permutations on $G(\tau, X)$ which are the same up to the choice of $m-1$ elements. Each of these pieces produces m unlabelled odd pieces by removing an element, and identifying $m-1$ elements again gives us all odd permutations on $G(\tau, X)$.

tions for odd n is now

$$\begin{aligned}\texttt{ODD SUM} &= \left(e^{S_{A_1}}\right)^{2k} \sum_{m=1}^{k} T_e(k,m) \left(\frac{e^{S_B} e^{S_{A_2}}}{e^{S_{A_1}}}\right)^m \\ &= \left(e^{S_{A_1}}\right)^{2k-1} e^{S_{A_2}} e^{S_B} {}_2F_1\left(1-2k, 1-k, 1; \frac{e^{S_B} e^{S_{A_2}}}{e^{S_{A_1}}}\right)\end{aligned} \tag{5.32}$$

As a sanity check for our counting functions $T_e(k,m)$ and $T_o(k,m)$, both $T_e(k,k)$ and $T_o(k,k)$ are equal to the symmetry factors for the pairwise connected geometries:

$$T_e(k,k) = C_k, \quad T_o(k,k) = (2k-1)C_{k-1} \tag{5.33}$$

and $T_e(k,1) = T_o(k,1) = 1$.

Therefore the ensemble averaged partially transposed density matrices are

$$\overline{\mathrm{Tr}(\rho_{A_1A_2}^{T_2})^{2k}} = \begin{cases} \frac{1}{\mathcal{N}^{2k}} e^{2k(S_{A_2}+S_B)+S_{A_1}} e^{S_{A_2}} {}_2F_1\left(1-k, -2k; 2; e^{S_{A_1}-S_{A_2}-S_B}\right), S_{A_1} < S_{A_2}+S_B \\ \frac{1}{\mathcal{N}^{2k}} e^{2kS_{A_1}+S_{A_2}+S_B} e^{S_{A_2}} {}_2F_1\left(1-k, -2k; 2; e^{S_{A_2}+S_B-S_{A_1}}\right), S_{A_1} > S_{A_2}+S_B \end{cases} \tag{5.34}$$

for even $n = 2k$ and

$$\overline{\mathrm{Tr}(\rho_{A_1A_2}^{T_2})^{2k-1}} = \begin{cases} \frac{1}{\mathcal{N}^{2k-1}} e^{(2k-1)(S_{A_2}+S_B)+S_{A_1}} {}_2F_1\left(1-2k, 1-k; 1; e^{S_{A_1}-S_{A_2}-S_B}\right), S_{A_1} < S_{A_2}+S_B \\ \frac{1}{\mathcal{N}^{2k-1}} e^{(2k-1)S_{A_1}+S_{A_2}+S_B} {}_2F_1\left(1-2k, 1-k; 1; e^{S_{A_2}+S_B-S_{A_1}}\right), S_{A_1} > S_{A_2}+S_B \end{cases} \tag{5.35}$$

for odd $n = 2k-1$.

5.3 Negativity Phase Transitions

We can use Eqs. (5.34) and (5.35) to understand the difference between the microcanonical and canonical Rényi negativities in a chaotic eigenstate, using much the same techniques as were used in [70]. We denote by f_{A_1} the volume fraction of A_1 such that the naïve phase transition happens at $f_{A_1} = 1/2$. We also denote the volume fraction of A_2 by f_{A_2} and use $f_A = f_{A_1} + f_{A_2}$ to denote the total volume fraction of system A.

We impose energy conservation in all three subsystems, such that our ansatz is for subsystem entropies is

$$\begin{aligned} S_{A_1}(E_{A_1}) &= f_{A_1} V s\left(\frac{E_{A_1}}{f_{A_1} V}\right) \\ S_{A_2}(E_{A_2}) &= f_{A_2} V s\left(\frac{E_{A_2}}{f_{A_2} V}\right) \\ S_B(E - E_{A_1} - E_{A_2}) &= (1 - f_A) V s\left(\frac{E - E_{A_1} - E_{A_2}}{(1 - f_A) V}\right). \end{aligned} \tag{5.36}$$

These again follow from ergodicity and imposing that the subsystem entropy is only a function of the subsystem energy density.

5.3.1 Comments on Our Ensemble Averaging

Unlike the case of Rényi entropy, the ensemble average over the partially transposed density matrix is not equivalent to upgrading the resummed traces (5.34) and (5.35) using the ansatz (5.36). The reason for this is that energy conservation between replicated subsystems for negativity forces "non-adjacent" subsystems to interact. The rules for energy conservation are outlined in [66][1]. For a given permutation, one can "follow the lines" of the three subsystems to see how the replicas interact. For an untransposed system, the constraints conspire such that a resolvent sum over diagrams holds away from the infinite temperature limit.

[1] We thank Jonah Kudler-Flam for discussions on this point and explaining his work.

This is no longer the case upon transposing. For simple permutations like $g = \mathbb{1}$ and $g = X$, imposing the constraints returns integrals similar to those in the Rényi entropy case. Things get more involved for general permutations on $G(\tau, X)$; the simplest permutations are a subset of our τ permutations, labelled τ_{ES} in [66]:

$$\tau_{ES} = (12)(34)\cdots(n-1\ n) \text{ or } (23)(45)\cdots(n\ 1) \tag{5.37}$$

These permutations require an integral over four subsystem energies, and the number of integrals only grows for arbitrary permutations on $G(\tau, X)$. This implies our ansatz (5.36) doesn't describe energy conservation described by disorder averaging over (5.14).

Given this obstruction, we make the choice to connect the replicas in a manner that reduces to the smallest number of integrals over subsystem energies. This has the advantage of allowing us to write a resolvent equation and resum the relevant permutations, while not having a correct interpretation as a trace-preserving energy flow between replicas. This produces some obvious pathologies, such as disagreement between the second even Rényi negativity and the second Rényi entropy, which must agree for a well-defined density matrix. However, as we'll see, even in this model one can reproduce some features of negativity seen in the gravitational model, namely large deviations from the thermodynamic answer for entanglement negativity and an enhanced correction for the partially transposed entropy.

5.3.2 Even Rényi Negativity

We'll start with studying the even Rényi negativities, from which the logarithmic negativity descends. Our expressions for the logarithms of the canonical ensemble and microcanonical

ensemble Rényi negativities using our previous ansatzes are as follows:

$$\begin{aligned}\overline{\mathcal{N}_{2k}} &= \frac{1}{\mathcal{N}^{2k}}\int dE_{A_1}dE_{A_2}e^{S_{A_1}(E_{A_1})+2S_{A_2}(E_{A_2})+S_B(E-E_{A_1}-E_{A_2})}G_k(f_{A_1},f_{A_2},E_{A_1},E_{A_2})\\ \mathcal{N}_{2k}^{MC} &= \frac{1}{\mathcal{N}^{2k}}\int dE_{A_1}dE_{A_2}e^{S_{A_1}(E_{A_1})+S_{A_2}(E_{A_2})+2k(S_{A_2}(E_{A_2})+S_B(E-E_{A_1}-E_{A_2}))},\end{aligned} \tag{5.38}$$

where the function $G_k(f_{A_1}, f_{A_2}, E_{A_1}, E_{A_2})$ is defined as the k-dependent part of Eq. (5.34)

$$\begin{aligned}&G_k(f_{A_1},f_{A_2},E_{A_1},E_{A_2}) =\\ &\begin{cases} e^{(2k-1)(S_{A_2}+S_B)}{}_2F_1\left(1-k,-2k;2;e^{S_{A_1}-S_{A_2}-S_B}\right), S_{A_1}<S_{A_2}+S_B\\ e^{(2k-1)S_{A_1}}{}_2F_1\left(1-k,-2k;2;e^{S_{A_2}+S_B-S_{A_1}}\right), S_{A_1}>S_{A_2}+S_B,\end{cases}\end{aligned} \tag{5.39}$$

and $\mathcal{N}$ (with no other sub/superscripts) is an overall normalization given by

$$\mathcal{N} = \int dE_{A_1}dE_{A_2}e^{S_{A_1}(E_{A_1})+S_{A_2}(E_{A_2})+S_B(E-E_{A_1}-E_{A_2})}. \tag{5.40}$$

Whenever unspecified, the subsystem entropies should now be understood to be valued at the subsystem energies, which we only omit for notational clarity. We write the difference between the logarithms of these quantities as

$$\log\overline{\mathcal{N}_{2k}} - \log\mathcal{N}_{2k}^{MC} \equiv \log\left(\frac{\int dE_{A_1}dE_{A_2}\exp(F_1(E_{A_1},E_{A_2}))}{\int dE_{A_1}dE_{A_2}\exp(F_2(E_{A_1},E_{A_2}))}\right), \tag{5.41}$$

where the functions $F_1(E_{A_1}, E_{A_2})$ and $F_2(E_{A_1}, E_{A_2})$ are defined via the corresponding integrands in Eq. (5.38). The strategy will be to find saddle points for $F_1(E_{A_1}, E_{A_2})$ and $F_2(E_{A_1}, E_{A_2})$ and use the relative behavior of those saddle points to determine the scaling of the correction at transition.

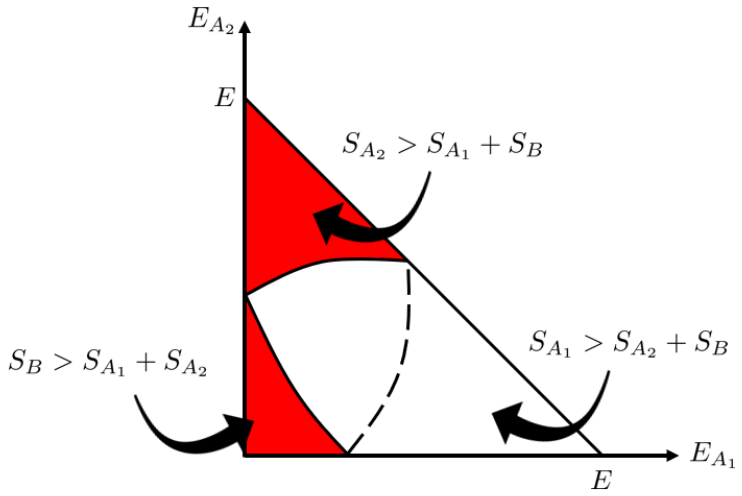

Figure 5.3: A schematic plot of regions (shaded in red) in the $E_{A_1} - E_{A_2}$ plane where our ansatz for the dominant sum over permutations does not hold. The lines separating the regions will depend sensitively on the form of $s(e)$ and the volume fractions of the subsystems.

We have two coupled saddle point equations for each both functions, which are given by

$$\begin{aligned}
s'\left(\frac{E_1^{(1)}}{f_{A_1}V}\right) &= s'\left(\frac{E - E_1^{(1)} - E_1^{(2)}}{(1-f_A)V}\right) - \frac{\partial_{E_{A_1}} G_k(f_{A_1}, f_{A_2}, E_1^{(1)}, E_1^{(2)})}{G_k(f_{A_1}, f_{A_2}, E_1^{(1)}, E_1^{(2)})} \\
2s'\left(\frac{E_1^{(2)}}{f_{A_2}V}\right) &= s'\left(\frac{E - E_1^{(1)} - E_1^{(2)}}{(1-f_A)V}\right) - \frac{\partial_{E_{A_2}} G_k(f_{A_1}, f_{A_2}, E_1^{(1)}, E_1^{(2)})}{G_k(f_{A_1}, f_{A_2}, E_1^{(1)}, E_1^{(2)})} \\
s'\left(\frac{E_2^{(1)}}{f_{A_1}V}\right) &= 2ks'\left(\frac{E - E_2^{(1)} - E_2^{(2)}}{(1-f_A)V}\right) \\
(2k+1)s'\left(\frac{E_2^{(2)}}{f_{A_2}V}\right) &= 2ks'\left(\frac{E - E_2^{(1)} - E_2^{(2)}}{(1-f_A)V}\right),
\end{aligned} \tag{5.42}$$

where the pair $\mathcal{E}_1 = (E_1^{(1)}, E_1^{(2)})$ denotes a saddle point for $F_1(E_{A_1}, E_{A_2})$, while $\mathcal{E}_2 = (E_2^{(1)}, E_2^{(2)})$ denotes the saddle point for $F_2(E_{A_1}, E_{A_2})$. As $F_2(E_{A_1}, E_{A_2})$ is a strictly concave function, there is only one global maximum. $F_1(E_{A_1}, E_{A_2})$ on the other hand can have two maxima, as $G_k(f_{A_1}, f_{A_2}, E_{A_1}, E_{A_2})$ is strictly nonmonotonic.

The first thing we have to be careful about is whether we are still within our regime of validity for probing the transition of interest. In the case of Rényi entropy, the fact that the

dominant contribution comes from non-crossing partitions was assumed to hold for all of parameter space, that is for all values of subsystem entropy. This can be traced back to the fact that the dominant permutations all lie on a single geodesic $G(\mathbb{1}, X)$. In our case, we're trying to probe the transition on one geodesic $G(\tau, X)$ while suppressing diagrams from other geodesics, which imposes some natural constraints on the size of our subsystems.

We are justified in only considering the diagrams from Section 5.2.2 only if the saddle point energies satisfy the conditions:

$$\begin{aligned} S_{A_2}(E_{1,2}^{(2)}) &< S_{A_1}(E_{1,2}^{(1)}) + S_B(E - E_{1,2}^{(1)} - E_{1,2}^{(2)}) \\ S_B(E - E_{1,2}^{(1)} - E_{1,2}^{(2)}) &< S_{A_1}(E_{1,2}^{(1)}) + S_{A_2}(E_{1,2}^{(2)}), \end{aligned} \tag{5.43}$$

such that all contributions from subleading permutations remain subleading. We include a rough phase diagram of the allowed region to explore in Figure 5.3. If the saddle point lies outside the allowed region, our answer for the dominant sum over permutations no longer holds, so we shouldn't try to explore those regions of phase space.

This means before attempting to compute corrections at transition for all subsystem volume fractions, we should derive some bounds on the regime of validity of our approximation. We'll make use of the following inequality:

$$S_{A_1}(E_{A_1}) + S_{A_2}(E_{A_2}) + S_B(E - E_{A_1} - E_{A_2}) \leq Vs\left(\frac{E}{V}\right), \tag{5.44}$$

which follows from the fact that our subsystem entropy function $s(e)$ is concave. Plugging in the saddle points and using the first constraint in Eq. (5.43) we can write

$$\begin{aligned} 2S_{A_2}(E_2^{(2)}) < S_{A_1}(E_2^{(1)}) + S_{A_2}(E_2^{(2)}) + S_B(E - E_2^{(1)} - E_2^{(2)}) &< Vs\left(\frac{E}{V}\right) \\ \Rightarrow S_{A_2}(E_2^{(2)}) &< \frac{V}{2}s\left(\frac{E}{V}\right). \end{aligned} \tag{5.45}$$

We can use this relation to find

$$S_{A_2}(E_2^{(2)}) = f_{A_2} s\left(\frac{E_2^{(2)}}{f_{A_2}V}\right) > f_{A_2} s\left(\frac{E_2^{(2)}}{V}\right)$$
$$\Rightarrow f_{A_2} s\left(\frac{E_2^{(2)}}{V}\right) < \frac{V}{2} s\left(\frac{E}{V}\right), \tag{5.46}$$

as $E_2^{(2)} < E$, a constraint on f_{A_2} which makes this true for all subsystem entropy densities is

$$f_{A_2} < 1/2. \tag{5.47}$$

Therefore our calculations are only valid when subsystem A_2 is less than half of the total system size. We can find a similar inequality on S_B using the second constraint in Eq. (5.43). We have

$$2S_B(E - E_2^{(1)} - E_2^{(2)}) < S_{A_1}(E_2^{(1)}) + S_{A_2}(E_2^{(2)}) + S_B(E - E_2^{(1)} - E_2^{(2)}) \leq Vs\left(\frac{E}{V}\right)$$
$$\Rightarrow S_B(E - E_2^{(1)} - E_2^{(2)}) < \frac{V}{2} s\left(\frac{E}{V}\right). \tag{5.48}$$

We can therefore write

$$S_B(E - E_2^{(1)} - E_2^{(2)}) = (1 - f_A)Vs\left(\frac{E - E_2^{(1)} - E_2^{(2)}}{(1 - f_A)V}\right)$$
$$> (1 - f_A)Vs\left(\frac{E - E_2^{(1)} - E_2^{(2)}}{V}\right)$$
$$\Rightarrow (1 - f_A)Vs\left(\frac{E - E_2^{(1)} - E_2^{(2)}}{V}\right) < \frac{V}{2} s\left(\frac{E}{V}\right). \tag{5.49}$$

Again, a result that makes this inequality true for all saddle point energies is

$$f_A > 1/2. \tag{5.50}$$

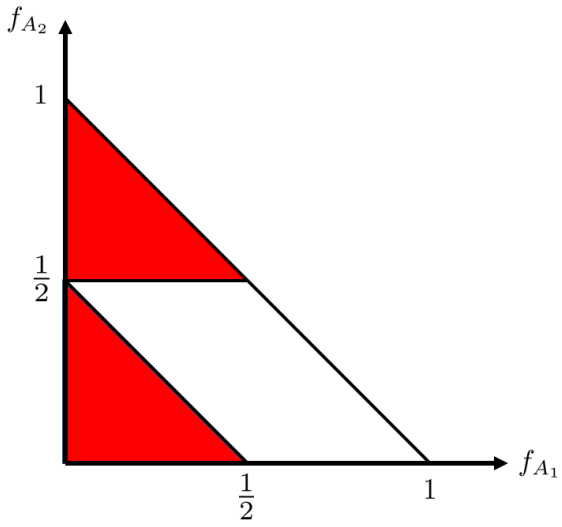

Figure 5.4: Excluded volume fractions from our analysis of the cyclic to pairwise phase transition. Describing the colored "forbidden" regions would require a sum over permutations we assert to be subdominant.

This ties together a nice family of restrictions: both subsystems A_2 and B have to have volume fraction less then half of the system. We illustrate these constraints in Figure 5.4. This makes some sense, as we want to probe transitions dominated by the behavior of A_1 relative to the rest of the system.

Another way of seeing there should be a restricted regime for our procedure is as follows: entanglement negativity is agnostic as to which subsystem A_1 or A_2 one applies the partial transpose to. This would of course result in an averaged density matrix trace symmetric under exchange of S_{A_1} and S_{A_2}, which our expressions (5.34) and (5.35) are not. However, by writing a resolvent equation valid only in a certain parameter regime, we can no longer comfortably integrate over all energies. This is an important point because the deviations from the feature-less case can in principle be of order the system size, and so corrections are not necessarily perturbative as they were assumed to be in [67].

We can, however, be comfortable in the validity of our calculation if the saddle points for $F_1(E_{A_1}, E_{A_2})$ and $F_2(E_{A_1}, E_{A_2})$ obey the conditions above, so restricting to the set of entropy

functions which satisfy Eq. (5.43), let's first look at the saddle point equations for $\mathcal{E}_2$. Setting the third and fourth equations equal yields

$$s'\left(\frac{E_2^{(1)}}{f_{A_1}V}\right) = (2k+1)s'\left(\frac{E_2^{(2)}}{f_{A_2}V}\right). \tag{5.51}$$

As $s'(e)$ is a monotonically decreasing function, for all $k > 0$ we have the inequality

$$E_2^{(2)} > \frac{f_{A_2}}{f_{A_1}}E_2^{(1)}. \tag{5.52}$$

We can use this inequality to write a simple inequality on $E_2^{(1)}$ by rewriting the $E_2^{(1)}$ saddle point equation as

$$s'\left(\frac{E_2^{(1)}}{f_{A_1}V}\right) > 2ks'\left(\frac{E - \frac{f_A}{f_{A_1}}E_2^{(1)}}{(1-f_A)V}\right). \tag{5.53}$$

Now we have an inequality which depends on k, as we can write

$$E_2^{(1)} < f_{A_1}E, \quad k \geq 1/2. \tag{5.54}$$

Note that this result is also valid for $k = 1/2$, as the relation (5.52) is a strict inequality which is never saturated for positive k. We can use a similar strategy to write an inequality for $E_2^{(2)}$. Rewriting the $E_2^{(2)}$ equation with (5.52) yields

$$(2k+1)s'\left(\frac{E_2^{(2)}}{f_{A_2}V}\right) < 2ks'\left(\frac{E - \frac{f_A}{f_{A_2}}E_2^{(2)}}{1-f_A}\right). \tag{5.55}$$

The resulting inequality has a slightly different k dependence:

$$E_2^{(2)} > f_{A_2}E, \quad k > 0. \tag{5.56}$$

The last inequalities we can write are those for the saddle point values of S_{A_1} and S_{A_2}:

$$\begin{aligned} S_{A_1}(E_2^{(1)}) &= f_{A_1} V s\left(\frac{E_2^{(1)}}{f_{A_1} V}\right) < f_{A_1} V s\left(\frac{E}{V}\right) \\ S_{A_2}(E_2^{(2)}) &= f_{A_2} V s\left(\frac{E_2^{(2)}}{f_{A_2} V}\right) > f_{A_2} V s\left(\frac{E}{V}\right). \end{aligned} \tag{5.57}$$

We'd like to find conditions on the hypergeometric being stuck on the first branch, i.e. $S_{A_1} < S_{A_2} + S_B$. This is guaranteed to happen if the weaker inequality $S_{A_1} < S_{A_2}$ is satisfied, which from Eq. (5.57) is necessarily true when

$$f_{A_2} > f_{A_1}. \tag{5.58}$$

If we assume $S_{A_1} < S_{A_2}$ for the $\mathcal{E}_1$ saddle point as well, the argument of the hypergeometric is exponentially suppressed and we can approximate it by

$${}_2F_1(1-k, -2k; 2; x) \approx 1 + k(k-1)x, \tag{5.59}$$

where the small parameter x is now

$$x \equiv e^{S_{A_1}(E_1^{(1)}) - S_{A_2}(E_1^{(2)}) - S_B(E - E_1^{(1)} - E_1^{(2)})}. \tag{5.60}$$

Under this assumption the saddle point equations for $\mathcal{E}_1$ and $\mathcal{E}_2$ are the same up to exponentially suppressed terms, and therefore the saddle points $\mathcal{E}_1$ and $\mathcal{E}_2$ are exponentially close. This leads to the following form of corrections to ETH:

$$\log \overline{\mathcal{N}_{2k}} - \log \mathcal{N}_{2k}^{MC} \propto \mathcal{O}(e^{-cV}), \quad k \geq 1/2, f_{A_2} > f_{A_1} \tag{5.61}$$

We can write a similar inequality for which $S_{A_1} < S_B$ is always satisfied. We recall the $E_2^{(1)}$

saddle point equation:

$$s'\left(\frac{E_2^{(1)}}{f_{A_1}}\right) = 2ks'\left(\frac{E - E_2^{(1)} - E_2^{(2)}}{(1-f_A)V}\right). \tag{5.62}$$

At $k = 1/2$ there's clearly an equality between the arguments of the functions on the right and left, so for $k \geq 1/2$ we have the inequality

$$\frac{E_2^{(1)}}{fV} \leq \frac{E - E_2^{(1)} - E_2^{(2)}}{(1-f_A)V}, \quad k \geq 1/2. \tag{5.63}$$

We'd like to satisfy the inequality $S_{A_1} < S_B$, or

$$f_{A_1} V s\left(\frac{E_2^{(1)}}{fV}\right) < (1-f_A)Vs\left(\frac{E - E_2^{(1)} - E_2^{(2)}}{(1-f_A)V}\right). \tag{5.64}$$

This is always satisfied if

$$f_{A_1} < 1 - f_A. \tag{5.65}$$

So far we have two constraints which carve out a corner of the phase space for all $k \geq 1/2$.

Now let's try to find a condition such that $S_{A_1} > S_{A_2} + S_B$. Using our previous ansatz this condition is written as

$$f_{A_1} s\left(\frac{E_2^{(1)}}{f_{A_1}V}\right) > f_{A_2} s\left(\frac{E_2^{(2)}}{f_{A_2}V}\right) + (1-f_A)s\left(\frac{E - E_2^{(1)} - E_2^{(2)}}{(1-f_A)V}\right). \tag{5.66}$$

For all $k > 0$ we can use Eq. (5.52) to rewrite this as

$$(f_{A_1} - f_{A_2})s\left(\frac{E_2^{(2)}}{f_{A_2}V}\right) > (1-f_A)s\left(\frac{E - E_2^{(1)} - E_2^{(2)}}{(1-f_A)V}\right). \tag{5.67}$$

Using the $E_2^{(2)}$ saddle point equation, there exists for $k > 0$:

$$\frac{E_2^{(2)}}{f_{A_2}} > \frac{E - E_2^{(1)} - E_2^{(2)}}{1 - f_A}. \tag{5.68}$$

Therefore, $S_{A_1} > S_{A_2} + S_B$ is always satisfied if

$$f_{A_1} - f_{A_2} > 1 - f_A \Rightarrow f_{A_1} > 1/2, \quad k > 0. \tag{5.69}$$

For these volume fractions the corrections to the Rényi negativity are extensive in the system size, as $\mathcal{E}_1$ and $\mathcal{E}_2$ have no relation:

$$\log \overline{\mathcal{N}_{2k}} - \log \mathcal{N}_{2k} \propto \mathcal{O}(V), \quad k > 0, f_{A_1} > 1/2. \tag{5.70}$$

We summarize the results so far in Figure 5.5. In that phase diagram, none of the boundaries should be though of as sharp, that is as Eq. (5.52) is never saturated for $k > 0$, neither are any constraints that depend on it. The interpolation between $\mathcal{O}(e^{-cV})$ corrections and $\mathcal{O}(V)$ corrections will happen somewhere in this "unknown region", though the only relevant point is that at $f_{A_1} = 1/2$ we should still be in a region with extensive corrections. In particular this implies the logarithmic negativity receives $\mathcal{O}(V)$ corrections, as was noted in [67].[2]

We won't comment on the case $k < 1/2$ for $f_{A_1} < 1/2$, though the expectation is that, like the $n < 1$ Rényi entropy, these measures always receive volume law corrections. It's also entirely possible the interpolating line continues moving towards the point $(0, 1/2)$, meaning there's some set of volume fractions for which arbitrarily small but positive k are well-approximated by ETH.

[2] At $k = 1$, the even Rényi negativity is equal to the second Rényi entropy $S_2(\rho_A)$, which for $f_{A_1} + f_{A_2} > 1/2$ is expected to always receive volume law corrections, which we don't see for all volume fractions. This could be a consequence of the restriction to a particular phase transition, but more likely is a result of the issues discussed in our ansatz above.

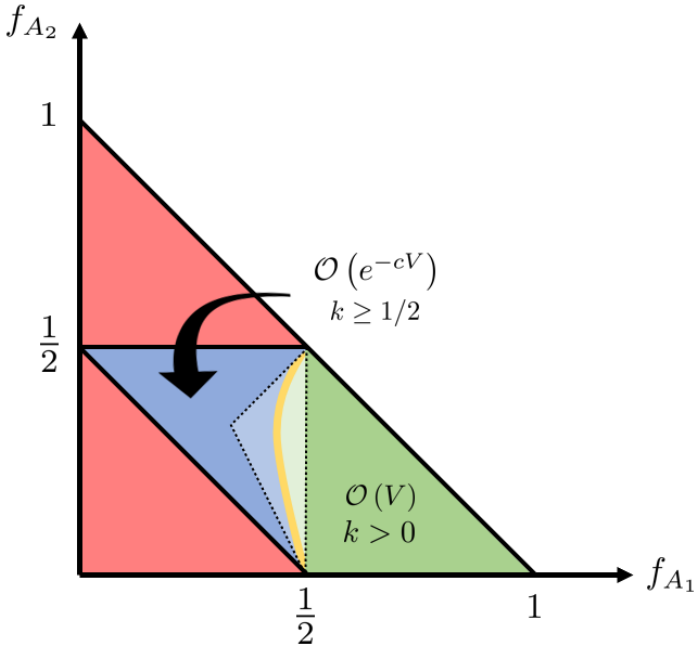

Figure 5.5: Phase diagram for corrections to even Rényi negativities. The concave region with $\mathcal{O}(e^{-cV})$ corrections comes from requiring $S_{A_1} < S_{A_2}$ and/or $S_{A_1} < S_B$. The $\mathcal{O}(V)$ region requires $S_{A_1} > S_{A_2} + S_B$. The interpolation between these regions will lie somewhere with $f_{A_1} < 1/2$ and is outlined by the dashed lines. The yellow curve represents a system specific boundary which will depend on k and potentially on the specifics of $s(e)$.

5.3.3 Odd Rényi Negativity

We can repeat the previous analysis for odd n. We have different expressions for the canonical and microcanonical Rényi negativities:

$$\begin{aligned}\log\overline{\mathcal{N}_{2k-1}} &= \frac{1}{\mathcal{N}_{2k-1}}\int dE_{A_1}dE_{A_2}e^{S_{A_1}(E_{A_1})+S_{A_2}(E_{A_2})+S_B(E-E_{A_1}-E_{A_2})}G_k(f_{A_1},f_{A_2},E_{A_1},E_{A_2})\\ \log\mathcal{N}^{MC}_{2k-1} &= \frac{1}{\mathcal{N}_{2k-1}}\int dE_{A_1}dE_{A_2}e^{S_{A_1}(E_{A_1})+(2k-1)(S_{A_2}(E_{A_2})+S_B(E-E_{A_1}-E_{A_2}))},\end{aligned} \tag{5.71}$$

where $G_k(f_{A_1},f_{A_2},E_{A_1},E_{A_2})$ is now defined by Eq. (5.35) as:

$$\begin{aligned}&G_k(f_{A_1},f_{A_2},E_{A_1},E_{A_2}) =\\ &\begin{cases} e^{(2k-2)(S_{A_2}+S_B)}{}_2F_1\left(1-k,1-2k;1;e^{S_{A_1}-S_{A_2}-S_B}\right), S_{A_1}<S_{A_2}+S_B\\ e^{(2k-2)S_{A_1}}{}_2F_1\left(1-2k,1-k;1;e^{S_{A_2}+S_B-S_{A_1}}\right), S_{A_1}>S_{A_2}+S_B.\end{cases}\end{aligned} \tag{5.72}$$

Again the subsystem entropies should be valued at their respective subsystem energies. Notably $\log\overline{\mathcal{N}_{2k-1}}$ enjoys a symmetry under $S_{A_1}\leftrightarrow S_{A_2}+S_B$. We again write the difference between the canonical and microcanonical answers as

$$\log\overline{\mathcal{N}_{2k-1}}-\log\mathcal{N}^{MC}_{2k-1}=\log\left(\frac{\int dE_{A_1}dE_{A_2}\exp(F_1(E_{A_1},E_{A_2}))}{\int dE_{A_1}dE_{A_2}\exp(F_2(E_{A_1},E_{A_2}))}\right) \tag{5.73}$$

and use the same ansatz (5.36) to write the saddle point equations for F_1 and F_2 as

$$\begin{aligned}
s'\left(\frac{E_1^{(1)}}{f_{A_1}V}\right) &= s'\left(\frac{E-E_1^{(1)}-E_1^{(2)}}{(1-f_A)V}\right) - \frac{\partial_{E_{A_1}} G_k(f_{A_1}, f_{A_2}, E_1^{(1)}, E_1^{(2)})}{G_k(f_{A_1}, f_{A_2}, E_1^{(1)}, E_1^{(2)})} \\
s'\left(\frac{E_1^{(2)}}{f_{A_2}V}\right) &= s'\left(\frac{E-E_1^{(1)}-E_1^{(2)}}{(1-f_A)V}\right) - \frac{\partial_{E_{A_2}} G_k(f_{A_1}, f_{A_2}, E_1^{(1)}, E_1^{(2)})}{G_k(f_{A_1}, f_{A_2}, E_1^{(1)}, E_1^{(2)})} \\
s'\left(\frac{E_2^{(1)}}{f_{A_1}V}\right) &= (2k-1)s'\left(\frac{E-E_2^{(1)}-E_2^{(2)}}{(1-f_A)V}\right) \\
s'\left(\frac{E_2^{(2)}}{f_{A_2}V}\right) &= s'\left(\frac{E-E_2^{(1)}-E_2^{(2)}}{(1-f_A)V}\right).
\end{aligned} \tag{5.74}$$

Let's again investigate the saddle point for F_2. We immediately see

$$\frac{E_2^{(2)}}{f_{A_2}} = \frac{E-E_2^{(1)}-E_2^{(2)}}{1-f_A} \tag{5.75}$$

for all k! This is a striking result, as it means we can write the sum of subsystem entropies in A_2 and B as

$$S_{A_2}(E_2^{(2)}) + S_B(E-E_2^{(1)}-E_2^{(2)}) \equiv S_{\overline{A_1}}(E_2^{(2)}) = (1-f_{A_1})s\left(\frac{E_2^{(2)}}{f_{A_2}V}\right) \tag{5.76}$$

This is important as for the odd Rényi negativity, S_{A_2} and S_B always appear summed, so if we're only interested in the leading saddle point approximation we can treat them as one subsystem entropy $S_{\overline{A_1}}$. As such we can rewrite the single saddle point equation as

$$s'\left(\frac{E_2^{(1)}}{f_{A_1}V}\right) = (2k-1)s'\left(\frac{E_2^{(2)}}{f_{A_2}V}\right). \tag{5.77}$$

At $k = 1$ we can exactly solve for the subsystem energies and they are, unsurprisingly, proportional to the volume fractions of their respective subsystems:

$$E_2^{(1)} = f_{A_1} E, \quad k = 1$$
$$E_2^{(2)} = f_{A_2} E, \quad k = 1. \tag{5.78}$$

When $k > 1$, we again have

$$E_2^{(2)} > \frac{f_{A_2}}{f_{A_1}} E_2^{(1)}, \tag{5.79}$$

which was true for general k in the even case. Similar inequalities on volume fraction hold in the odd case; we still have

$$E_2^{(1)} < f_{A_1} E, \quad k > 1$$
$$E_2^{(2)} > f_{A_2} E, \quad k > 1. \tag{5.80}$$

From this the inequality $S_{A_1} < S_{\overline{A_1}}$ is clearly satisfied when

$$f_{A_1} < 1/2, \tag{5.81}$$

and corrections are exponentially suppressed. For $f_{A_1} > 1/2$, this won't be true generically and the corrections are extensive.

We can also say interesting things about $k < 1$. In this case the inequalities are flipped:

$$E_2^{(1)} > f_{A_1} E, \quad k < 1$$
$$E_2^{(2)} < f_{A_2} E, \quad k < 1$$
$$E_2^{(2)} < \frac{f_{A_2}}{f_{A_1}} E_2^{(1)}. \tag{5.82}$$

We can check where $S_{A_1} > S_{\overline{A_1}}$. From the inequality (5.82) we have

$$\begin{aligned} S_{A_1}(E_2^{(1)}) &= f_{A_1} V s\left(\frac{E_2^{(1)}}{f_{A_1} V}\right) > f_{A_1} V s\left(\frac{E}{V}\right) \\ S_{\overline{A_1}}(E_2^{(2)}) &= (1-f_{A_1}) V s\left(\frac{E_2^{(2)}}{f_{A_2} V}\right) < (1-f_{A_1}) V s\left(\frac{E}{V}\right). \end{aligned} \tag{5.83}$$

We see that $S_{A_1} > S_{\overline{A_1}}$ is guaranteed to be satisfied if $f_{A_1} > 1/2$, and indeed there is no generic behavior for $f_{A_1} < 1/2$. Thus the corrections are extensive for all volume fractions for $k < 1$.

5.3.4 Odd Rényi Negativity at Transition

We would like to study this case in analogy with the entanglement entropy, for reasons that will be clear shortly. Let's follow the same procedure explained in [70] of dividing F_1 into two pieces, F_{dom} and F_Δ, defined as

$$\begin{aligned} F_{\text{dom}} &= S_{A_1}(E_{A_1}) + S_{A_2}(E_{A_2}) + S_B(E - E_{A_1} - E_{A_2}) \\ &\quad + (2k-2)\text{max}\{S_{A_1}(E_{A_1}), S_{A_2}(E_{A_2}) + S_B(E - E_{A_1} - E_{A_2})\} \\ F_\Delta &= \log {}_2F_1\left(1-2k, 1-k; 1; e^{-|S_{A_1}(E_{A_1}) - S_{A_2}(E_{A_2}) - S_B(E-E_{A_1}-E_{A_2})|}\right). \end{aligned} \tag{5.84}$$

That is, we take the dominant contribution and relegate the subleading contributions to a term bounded by $\mathcal{O}(1)$ in volume factors:

$$1 \leq e^{F_\Delta} \leq a_k, \quad a_k \equiv \binom{3k-2}{k-1} = \frac{\Gamma(3k-1)}{\Gamma(k)\Gamma(2k)} = 1 + (k-1) + \mathcal{O}(k-1)^2. \tag{5.85}$$

The averaged Rényi negativity, with a $\frac{1}{2k-2}$ factor which will be important later, can be rewritten as

$$\frac{1}{2k-2} \log \overline{\mathcal{N}_{2k-1}} = \frac{1}{2k-2} \log \left(\frac{1}{\mathcal{N}_{2k-1}} \int dE_{A_1} dE_{A_2} e^{F_{\text{dom}} + F_\Delta}\right), \tag{5.86}$$

and we can bound $\log \overline{\mathcal{N}_{2k-1}}$ via

$$\log \overline{\mathcal{N}_{2k-1}} - \log \mathcal{N}_{2k-1}^{\text{dom}} \leq \frac{1}{2} + \mathcal{O}(k-1). \tag{5.87}$$

As such $\mathcal{N}_{2k-1}^{\text{dom}}$ is enough to look for corrections larger than $\mathcal{O}(1)$.

Unlike the Rényi entropy, at $f = 1/2$ there's no obvious reflection symmetry of the energies in F_{dom}, and indeed we don't find one numerically. There is, however, a symmetry in the saddle points, which we'll argue for as follows. Call the two saddle points for F_{dom} (or F_1, it makes no difference here) $\mathcal{E}_1^{(a)} = (E_1^{(1,a)}, E_1^{(2,a)})$ and $\mathcal{E}_1^{(b)} = (E_1^{(1,b)}, E_1^{(2,b)})$. Under the exchange $S_{A_1} \leftrightarrow S_{\overline{A}_1}$, the saddles are swapped due to the symmetry of the odd Rényi negativity. It's clear then at $f_{A_1} = 1/2$ there exists the equivalence

$$\begin{aligned} \frac{E_1^{(1,a)}}{f_{A_1}} &= \frac{E_1^{(2,b)}}{f_{A_2}} \\ \frac{E_1^{(1,b)}}{f_{A_2}} &= \frac{E_1^{(2,a)}}{f_{A_2}}. \end{aligned} \tag{5.88}$$

This means that the two saddle points contribute with equal magnitude, which contributes an $\mathcal{O}(1)$ factor to the difference between the canonical and microcanonical negativities:

$$\frac{1}{2k-2}\left(\log \mathcal{N}_{2k-1}^{\text{dom}} - \log \mathcal{N}_{2k-1}^{MC}\right) = \frac{\log 2}{2-2k} \sim \mathcal{O}(1) \tag{5.89}$$

However, as in the case of von Neumann entropy, there is a subtlety related to the fact that the two saddles collide in the limit $k \to 1$, i.e. the partially transposed entropy. As they collide, there is an emergent region between the saddles which contributes to the integral, so we can't treat the presence of multiple equivalent saddles at leading order, we must integrate over the interpolating region. We show a plot of this phenomenon in Figure 5.6. Let's solve the F_2 saddle point equations perturbatively in $\delta \equiv 2k-2$. The $E_2^{(1)}$ saddle point equation (5.77)

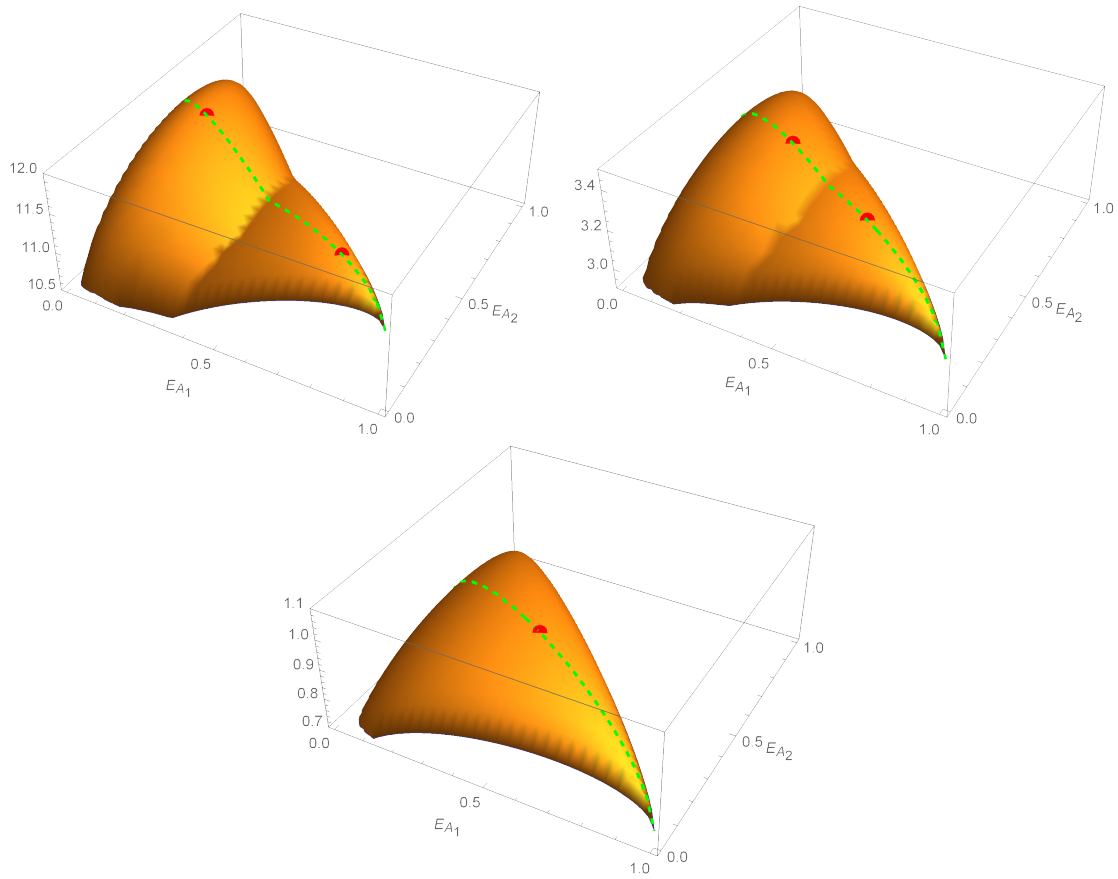

Figure 5.6: Plots of $F_1(E_{A_1}, E_{A_2})$ at phase transition. We've set $E = V = 1, f_{A_1} = 1/2$, and $f_{A_2} = 3/10$. For large k (upper left), the two saddle points are well-separated and can be treated separately. As we decrease k (upper right) the saddle points approach one another and produce an emergent flat region. At exactly $k = 1$ (bottom) the saddle points coincide at $(f_{A_1}E, f_{A_2}E)$. The dotted line connecting the saddle points is given by $E_{A_2} = -2f_{A_2}(E_{A_1} - E)$; all saddles at $f_{A_1} = 1/2$ lie along this line.

becomes

$$s'\left(\frac{E_2^{(1)}}{f_{A_1}V}\right) = (1+\delta)s'\left(\frac{E_2^{(2)}}{f_{A_2}V}\right) \approx s'\left(\frac{E_2^{(2)}}{f_{A_2}V} + \delta\frac{s'\left(E/V\right)}{s''\left(E/V\right)}\right), \tag{5.90}$$

where we've again used that $E_2^{(2)} = f_{A_2}E$. Combining this with the unchanged equality (5.75) and plugging in $f_{A_1} = 1/2$ yields

$$\begin{aligned} E_2^{(1)} &= \frac{E}{2} + \frac{V\delta}{4}\frac{s'(E/V)}{s''(E/V)} \\ E_2^{(2)} &= f_{A_2}E - \frac{f_{A_2}V\delta}{2}\frac{s'(E/V)}{s''(E/V)} \end{aligned} \tag{5.91}$$

From this we can write our subsystem entropies S_{A_1} and $S_{\overline{A_1}}$ in the familiar form

$$\begin{aligned} S_{A_1}(E_2^{(1)}) &= \frac{1}{2}s\left(E + \frac{V\delta}{2}\frac{s'(E/V)}{s''(E/V)}\right) \\ S_{\overline{A_1}}(E_2^{(2)}) &= \frac{1}{2}s\left(E - \frac{V\delta}{2}\frac{s'(E/V)}{s''(E/V)}\right) \end{aligned} \tag{5.92}$$

What happens as $k \to 1$ for the odd Rényi negativity is precisely the same as what happens for the $n \to 1$ von Neumann entropy, namely that the F_Δ term "fills in" the space between the two saddles. The only difference is that this flat direction runs between two saddles separated along a line in the $E_{A_1} - E_{A_2}$ plane specified by f_{A_2}. The rest of the calculation is completely unchanged from that of the von Neumann entropy, and there is an enhanced correction exactly of the same form:

$$\overline{S^{T_2}} - S_{MC}^{T_2} = -\sqrt{\frac{C_V}{2\pi}} + \mathcal{O}(\delta) \sim \mathcal{O}(\sqrt{V}) \tag{5.93}$$

In [67], it was noted that a naïve calculation shows the partially transposed entropy receives $\mathcal{O}(\sqrt{V})$ corrections, but a more accurate analysis shows it receives $\mathcal{O}(V)$ corrections. It would be interesting to understand the difference between our calculation and theirs.[3]

[3] A possible resolution is that our calculation was done at fixed f_{A_2}, roughly the same as fixing k_2 in [67]. Only when $k = k_1k_2$ was fixed, similar to fixing f_A, do they see $\mathcal{O}(V)$ corrections.

5.4 Discussion

In this work we've studied a class of tripartite entanglement measures, the Rényi negativities, in a toy model of a chaotic eigenstate. We've resummed the relevant non-crossing permutations obtained via Wick contractions relevant at the transition of interest and studied the corrections to the dominant microcanonical saddle while imposing energy conservation only within each copy in our ensemble average.

With this simplification the main takeaway is as follows: logarithmic negativity and its Rényi generalizations thereof are not always "good" chaotic observables in the sense that their fluctuations (the difference between the canonical and microcanonical expectation values) are often of the same order as the quantities themselves, implying they are not self-averaging for all volume fractions. We've shown this is the case for the even Rényi negativity at transition, as well as for both even and odd Rényi negativities for $f_{A_1} > 1/2$. In particular we've shown that odd Rényi negativity behaves mostly the same as Rényi entropy at the τ to X transition, exhibiting a $\mathcal{O}(\sqrt{V})$ enhanced correction at exactly $k = 1$. One surprising outcome is that, for both Rényi negativities, canonical typicality holds in some cases where the partially transposed density matrix is defined on a subsystem A_1A_2 larger than half of the total system.

Chapter 6

Future Directions

The work presented in Chapter 2 gives way to a few possible directions for future work. First, numerical testing of non-Abelian ETH are called upon to validate our theoretical results. It would also be instructive to see theoretical results derived for systems with other conserved non-Abelian charges. Numerical evidence for a variety of quantum chaotic systems with conserved non-Abelian charges would fortify our claim of non-Abelian ETH to suffice as a full extension of standard ETH.

The question of what connections, if any, non-Abelian ETH and quantum many-body scars (QMBS) have is also worth exploring. QMBS arise due to non-Abelian symmetries (spectrum generating algebras) [16]. These spectrum generating algebras create a few[1] states which violate ETH. As mentioned in the chapter, the possibility for anomalous thermalization is remarked in [19]. This depends on two things: specific initial states and sub-extensive scalings of an observable. Perhaps there could be a link between QMBS and these initial states.

The results of Chapter 3 pave the way for understanding the spectra of a single-spin-component operator in truly correlated systems. The spectra found in [35] for a single-spin-component operator seems to take on the form of a correlated centered Jacobi ensemble. Gener-

[1] A set of measure zero in the thermodynamic limit.

ally, correlated Jacobi ensembles do not have an analytical form, regardless of their correlation structure [80]. Nevertheless, it would be incredibly illuminating to see if information about the correlation structure between energy states in a physical system could be extracted by analyzing deviations from our benchmark. This could, perhaps, come from either analytical or numerical methods.

The possible directions for the work present in Chapter 4 are a bit more vague and broad. QFI has been used in many different contexts. Most work involving QFI presents results based on performing a local unitary transformation on an initial state. It would be interesting to see how results differ, in any context, if one considers the other protocols described here. One example is measuring multipartite entanglement via QFI in a system that has thermalized. Considering a local unitary operation, [42] gives a bound on n-particle entanglement. Analyzing how these different protocols change the resulting entanglement warrants exploration.

Finally, we discuss some extensions to the work of Chapter 5. First, our simplification yielded results close to that of [70] and it would be interesting to be able to give some physical interpretation to it. This should be followed up by finding a tractable way of conducting a more detailed analysis without the simplification of energy conservation within each copy in our ensemble. It would be illuminating to see the corrections to our results from imposing energy conservation between replicas as described in [66], and to understand if our simplified ansatz produces similar corrections at transition.

More generally, a necessary restriction in our analysis is summing only over a subset of all relevant permutations near a particular phase transition. It would be useful to find a closed-form expression for the moments of a block transposed Wishart matrix without these assumptions, which would involve finding a closed form solution to the recursion relation in [75]. This would be especially nice as we could probe the region $f_A < 1/2$, which is where one could expect ETH to hold as the partially transposed density matrix is defined on less than half of the total system.

A technical point in our analysis was the use of 2-Dyck paths and 2-Narayana numbers, as opposed to (1-)Dyck paths which appear in the calculation of entanglement entropy. It is possible some further generalization of Narayana numbers (as in e.g. [78]) will be relevant for calculating transitions in higher-party entanglement measures in a similar model.

So far, we have only discussed Rényi negativity, but there exists a family of holographically inspired measures termed "refined" Rényi negativities, which are given by

$$S^{T_2(n)}(\rho_{A_1A_2}) = -n^2\partial_n\left(\frac{1}{n}\log\mathcal{N}_n^{(\text{odd/even})}(\rho_{A_1A_2})\right). \tag{6.1}$$

We have not touched on the structure of transitions in these measures, but they could presumably be treated in the same way we have presented. Of particular interest is the refined Rényi 2-negativity $S^{T_2(2)}$, the $n \to 2$ limit of the even refined Rényi entropy. This quantity is explicitly given by

$$S^{T_2(2)} = -\lim_{m\to 1} m^2\partial_m\left(\frac{1}{m}\log\mathcal{N}_{2m}^{(\text{even})}\right) = -\sum_i \frac{\lambda_i^2}{\sum_j\lambda_j^2}\log\left(\frac{\lambda_i^2}{\sum_j\lambda_j^2}\right) \tag{6.2}$$

which is the von Neumann entropy of the normalized density matrix $\left(\rho_{A_1A_2}^{T_2}\right)^2$. Consequently, the expectation is that the corrections will be $\mathcal{O}(\sqrt{V})$, which is indeed what is seen in the gravitational setting. It would be nice to derive this relation from our formalism.

Additionally, this formalism could be applied to study the reflected entropy [81] and its Rényi generalizations thereof [82, 83, 84]. Reflected entropy has been studied in a similar gravitational system [83] and was shown to have $\mathcal{O}(\sqrt{V})$ corrections at transition, as in the case of the von Neumann entropy, derived via a resolvent calculation. Presumably the relevant permutations could be enumerated and the corrections calculated as we've done in this work.

We only considered the case where energy is conserved in all three subsystems. The authors of [66] consider some cases in a similar model where some subsystems are fixed at infinite

temperature, which would correspond to freezing the density of states in those subsystems; it would be interesting to understand to what extent this changes our results.

The rapid progress in technology has made it increasingly realistic to construct and manipulate quantum mechanical systems. This development necessitates further advancements in the study of quantum chaos and the eigenstate thermalization hypothesis. By exploring these areas, we can uncover additional universal properties of quantum chaotic systems, enhancing our understanding of the fundamental principles that govern them. As we delve deeper into this fascinating realm, new insights and discoveries await, promising exciting avenues for future research and applications.

Bibliography

[1] E. P. Wigner, *On the distribution of the roots of certain symmetric matrices*, *Annals of Mathematics* **67** (1958) 325.

[2] F. J. Dyson, *Statistical theory of the energy levels of complex systems. i*, *Journal of Mathematical Physics* **3** (1962), no. 1 140–156, [doi.org/10.1063/1.1703773].

[3] R. U. Haq, A. Pandey, and O. Bohigas, *Fluctuation properties of nuclear energy levels: Do theory and experiment agree?*, *Phys. Rev. Lett.* **48** (Apr, 1982) 1086–1089.

[4] O. Bohigas, M. J. Giannoni, and C. Schmit, *Characterization of chaotic quantum spectra and universality of level fluctuation laws*, *Phys. Rev. Lett.* **52** (Jan, 1984) 1–4.

[5] H. Friedrich and H. Wintgen, *The hydrogen atom in a uniform magnetic field — an example of chaos*, *Physics Reports* **183** (1989), no. 2 37–79.

[6] R. A. Jalabert, A. D. Stone, and Y. Alhassid, *Statistical theory of coulomb blockade oscillations: Quantum chaos in quantum dots*, *Phys. Rev. Lett.* **68** (Jun, 1992) 3468–3471.

[7] C. M. Marcus, A. J. Rimberg, R. M. Westervelt, P. F. Hopkins, and A. C. Gossard, *Conductance fluctuations and chaotic scattering in ballistic microstructures*, *Phys. Rev. Lett.* **69** (Jul, 1992) 506–509.

[8] V. V. Flambaum, A. A. Gribakina, G. F. Gribakin, and M. G. Kozlov, *Structure of compound states in the chaotic spectrum of the ce atom: Localization properties, matrix elements, and enhancement of weak perturbations*, *Phys. Rev. A* **50** (Jul, 1994) 267–296.

[9] G. Montambaux, D. Poilblanc, J. Bellissard, and C. Sire, *Quantum chaos in spin-fermion models*, *Phys. Rev. Lett.* **70** (Jan, 1993) 497–500.

[10] J. M. Deutsch, *Quantum statistical mechanics in a closed system*, *Phys. Rev. A* **43** (Feb, 1991) 2046–2049.

[11] M. V. Berry, *Regular and irregular semiclassical wavefunctions*, *Journal of Physics A: Mathematical and General* **10** (dec, 1977) 2083.

[12] M. Srednicki, *Chaos and quantum thermalization*, *Physical Review E* **50** (Aug, 1994) 888–901.

[13] M. Srednicki, *The approach to thermal equilibrium in quantized chaotic systems*, *Journal of Physics A: Mathematical and General* **32** (Jan, 1999) 1163–1175.

[14] M. Rigol, V. Dunjko, V. Yurovsky, and M. Olshanii, *Relaxation in a completely integrable many-body quantum system: Aniab initio/istudy of the dynamics of the highly excited states of 1d lattice hard-core bosons*, *Physical Review Letters* **98** (feb, 2007).

[15] D. A. Abanin, E. Altman, I. Bloch, and M. Serbyn, *Colloquium: Many-body localization, thermalization, and entanglement*, *Rev. Mod. Phys.* **91** (May, 2019) 021001.

[16] S. Moudgalya, B. A. Bernevig, and N. Regnault, *Quantum many-body scars and hilbert space fragmentation: a review of exact results*, *Reports on Progress in Physics* **85** (jul, 2022) 086501.

[17] V. Khemani, M. Hermele, and R. Nandkishore, *Localization from hilbert space shattering: From theory to physical realizations*, *Phys. Rev. B* **101** (May, 2020) 174204.

[18] T. Kinoshita, T. Wenger, and D. Weiss, *A quantum newton's cradle*, *Nature* **440** (05, 2006) 900–3.

[19] C. Murthy, A. Babakhani, F. Iniguez, M. Srednicki, and N. Yunger Halpern, *Non-abelian eigenstate thermalization hypothesis*, *Phys. Rev. Lett.* **130** (Apr, 2023) 140402.

[20] M. Pandey, P. W. Claeys, D. K. Campbell, A. Polkovnikov, and D. Sels, *Adiabatic eigenstate deformations as a sensitive probe for quantum chaos*, *Physical Review X* **10** (Oct, 2020).

[21] K. Kudo and T. Deguchi, *Level statistics of XXZ spin chains with discrete symmetries: Analysis through finite-size effects*, *Journal of the Physical Society of Japan* **74** (jul, 2005) 1992–2000.

[22] L. F. Santos, *Transport and control in one-dimensional systems*, *Journal of Mathematical Physics* **50** (sep, 2009) 095211.

[23] L. F. Santos and M. Rigol, *Onset of quantum chaos in one-dimensional bosonic and fermionic systems and its relation to thermalization*, *Phys. Rev. E* **81** (Mar, 2010) 036206.

[24] Y. Y. Atas, E. Bogomolny, O. Giraud, and G. Roux, *Distribution of the ratio of consecutive level spacings in random matrix ensembles*, *Physical Review Letters* **110** (Feb, 2013).

[25] D. Kapec, R. Mahajan, and D. Stanford, *Matrix ensembles with global symmetries and 't hooft anomalies from 2d gauge theory*, *Journal of High Energy Physics* **2020** (apr, 2020).

[26] N. Y. Halpern, P. Faist, J. Oppenheim, and A. Winter, *Microcanonical and resource-theoretic derivations of the thermal state of a quantum system with noncommuting charges*, *Nature Communications* **7** (jul, 2016).

[27] N. Y. Halpern, M. E. Beverland, and A. Kalev, *Noncommuting conserved charges in quantum many-body thermalization*, *Physical Review E* **101** (apr, 2020).

[28] R. Shankar, *Principles of Quantum Mechanics*. Springer, New York, NY, 2nd ed., 2008.

[29] A. Bohm, *Quantum mechanics: Foundations and Applications*. Springer, Berlin, Heidelberg, 2nd ed., 1986.

[30] M. Srednicki, *Thermal fluctuations in quantized chaotic systems*, *J. Phys. A: Math. Gen.* **29** (Feb, 1996) L75–L79.

[31] M. Rigol, V. Dunjko, and M. Olshanii, *Thermalization and its mechanism for generic isolated quantum systems*, *Nature* **452** (Apr, 2008) 854.

[32] L. D'Alessio, Y. Kafri, A. Polkovnikov, and M. Rigol, *From quantum chaos and eigenstate thermalization to statistical mechanics and thermodynamics*, *Adv. Phys.* **65** (2016), no. 3 239–362.

[33] J. M. Deutsch, *Eigenstate thermalization hypothesis*, *Rep. Prog. Phys.* **81** (Jul, 2018) 082001.

[34] L. Foini and J. Kurchan, *Eigenstate thermalization hypothesis and out of time order correlators*, *Phys. Rev. E* **99** (2019), no. 4 042139.

[35] J. Richter, A. Dymarsky, R. Steinigeweg, and J. Gemmer, *Eigenstate thermalization hypothesis beyond standard indicators: Emergence of random-matrix behavior at small frequencies*, *Phys. Rev. E* **102** (Oct, 2020) 042127.

[36] S. Pappalardi, L. Foini, and J. Kurchan, *Microcanonical windows on quantum operators*, 2023.

[37] B. Collins, *Product of random projections, jacobi ensembles and universality problems arising from free probability*, *Probability Theory and Related Fields* **133** (2005), no. 3 315–344.

[38] M. L. Mehta, *Random Matrices*. Elsevier, Amsterdam, 3rd ed., 2004.

[39] T.-C. Lu and T. Grover, *Renyi entropy of chaotic eigenstates*, *Physical Review E* **99** (mar, 2019).

[40] J. R. Garrison and T. Grover, *Does a single eigenstate encode the full hamiltonian?*, *Phys. Rev. X* **8** (Apr, 2018) 021026.

[41] J. Liu, H. Yuan, X.-M. Lu, and X. Wang, *Quantum fisher information matrix and multiparameter estimation*, *Journal of Physics A: Mathematical and Theoretical* **53** (dec, 2019) 023001.

[42] P. Hauke, M. Heyl, L. Tagliacozzo, and P. Zoller, *Measuring multipartite entanglement through dynamic susceptibilities*, *Nature Physics* **12** (2016), no. 8 778–782.

[43] M. Brenes, S. Pappalardi, J. Goold, and A. Silva, *Multipartite entanglement structure in the eigenstate thermalization hypothesis*, *Physical Review Letters* **124** (jan, 2020).

[44] S. Pappalardi, A. Russomanno, A. Silva, and R. Fazio, *Multipartite entanglement after a quantum quench*, *Journal of Statistical Mechanics: Theory and Experiment* **2017** (may, 2017) 053104.

[45] J. Liu, X.-X. Jing, W. Zhong, and X.-G. Wang, *Quantum fisher information for density matrices with arbitrary ranks*, *Communications in Theoretical Physics* **61** (jan, 2014) 45–50.

[46] M. Pandey, P. W. Claeys, D. K. Campbell, A. Polkovnikov, and D. Sels, *Adiabatic eigenstate deformations as a sensitive probe for quantum chaos*, *Physical Review X* **10** (oct, 2020).

[47] R. M. Wilcox, *Exponential operators and parameter differentiation in quantum physics*, *Journal of Mathematical Physics* **8** (1967), no. 4 962–982.

[48] C. Murthy and M. Srednicki, *Bounds on chaos from the eigenstate thermalization hypothesis*, *Physical Review Letters* **123** (dec, 2019).

[49] Q. Quan, H. Zhu, H. Fan, and W.-L. Yang, *Einstein-podolsky-rosen correlations and bell correlations in the simplest scenario*, *Physical Review A* **95** (jun, 2017).

[50] L. Gurvits, *Classical complexity and quantum entanglement*, *Journal of Computer and System Sciences* **69** (2004), no. 3 448–484. Special Issue on STOC 2003.

[51] G. Vidal and R. Werner, *Computable measure of entanglement*, *Phys. Rev. A* **65** (2002) 032314, [quant-ph/0102117].

[52] M. B. Plenio and S. Virmani, *An Introduction to entanglement measures*, *Quant. Inf. Comput.* **7** (2007) 1–51, [quant-ph/0504163].

[53] V. Eisler and Z. Zimborás, *On the partial transpose of fermionic gaussian states*, *New Journal of Physics* **17** (may, 2015) 053048.

[54] C. D. Nobili, A. Coser, and E. Tonni, *Entanglement negativity in a two dimensional harmonic lattice: area law and corner contributions*, *Journal of Statistical Mechanics: Theory and Experiment* **2016** (aug, 2016) 083102.

[55] D. Bianchini and O. A. Castro-Alvaredo, *Branch point twist field correlators in the massive free boson theory*, *Nuclear Physics B* **913** (2016) 879–911.

[56] V. Eisler and Z. Zimborás, *Entanglement negativity in two-dimensional free lattice models*, *Phys. Rev. B* **93** (Mar, 2016) 115148.

[57] H. Shapourian, K. Shiozaki, and S. Ryu, *Partial time-reversal transformation and entanglement negativity in fermionic systems*, *Phys. Rev. B* **95** (Apr, 2017) 165101.

[58] P. Calabrese, J. Cardy, and E. Tonni, *Entanglement negativity in quantum field theory*, *Phys. Rev. Lett.* **109** (Sep, 2012) 130502.

[59] P. Calabrese, J. Cardy, and E. Tonni, *Finite temperature entanglement negativity in conformal field theory*, *Journal of Physics A: Mathematical and Theoretical* **48** (dec, 2014) 015006.

[60] C. D. Nobili, A. Coser, and E. Tonni, *Entanglement entropy and negativity of disjoint intervals in cft: some numerical extrapolations*, *Journal of Statistical Mechanics: Theory and Experiment* **2015** (jun, 2015) P06021.

[61] H. Wichterich, J. Molina-Vilaplana, and S. Bose, *Scaling of entanglement between separated blocks in spin chains at criticality*, *Phys. Rev. A* **80** (Jul, 2009) 010304.

[62] P. Ruggiero, V. Alba, and P. Calabrese, *Entanglement negativity in random spin chains*, *Phys. Rev. B* **94** (Jul, 2016) 035152.

[63] Y. A. Lee and G. Vidal, *Entanglement negativity and topological order*, *Phys. Rev. A* **88** (Oct, 2013) 042318.

[64] C. Castelnovo, *Negativity and topological order in the toric code*, *Phys. Rev. A* **88** (Oct, 2013) 042319.

[65] T.-C. Lu and T. Grover, *Entanglement transitions as a probe of quasiparticles and quantum thermalization*, *Physical Review B* **102** (dec, 2020).

[66] S. Vardhan, J. Kudler-Flam, H. Shapourian, and H. Liu, *Mixed-state entanglement and information recovery in thermalized states and evaporating black holes*, *Journal of High Energy Physics* **2023** (jan, 2023).

[67] X. Dong, S. McBride, and W. W. Weng, *Replica Wormholes and Holographic Entanglement Negativity*, arXiv:2110.1194.

[68] L. Vidmar and M. Rigol, *Entanglement entropy of eigenstates of quantum chaotic hamiltonians*, *Physical Review Letters* **119** (nov, 2017).

[69] C. Murthy and M. Srednicki, *Structure of chaotic eigenstates and their entanglement entropy*, *Phys. Rev. E* **100** (2019), no. 2 022131, [arXiv:1906.0429].

[70] X. Dong and H. Wang, *Enhanced corrections near holographic entanglement transitions: a chaotic case study*, *JHEP* **11** (2020) 007, [arXiv:2006.1005].

[71] M. Plenio, *Logarithmic Negativity: A Full Entanglement Monotone That is not Convex*, *Phys. Rev. Lett.* **95** (2005), no. 9 090503, [quant-ph/0505071].

[72] K. Audenaert, M. Plenio, and J. Eisert, *Entanglement cost under positive-partial-transpose-preserving operations*, *Phys. Rev. Lett.* **90** (2003), no. 2 027901.

[73] A. Peres, *Separability criterion for density matrices*, *Phys. Rev. Lett.* **77** (1996) 1413–1415, [quant-ph/9604005].

[74] J. M. Deutsch, *Thermodynamic entropy of a many-body energy eigenstate*, *New Journal of Physics* **12** (jul, 2010) 075021.

[75] T. Banica and I. Nechita, *Asymptotic eigenvalue distributions of block-transposed wishart matrices*, *Journal of Theoretical Probability* **26** (2013), no. 3 855–869, [arXiv:1105.2556].

[76] H. Shapourian, S. Liu, J. Kudler-Flam, and A. Vishwanath, *Entanglement Negativity Spectrum of Random Mixed States: A Diagrammatic Approach*, *PRX Quantum* **2** (2021), no. 3 030347, [arXiv:2011.0127].

[77] E. Brezin, C. Itzykson, G. Parisi, and J. B. Zuber, *Planar Diagrams*, *Commun. Math. Phys.* **59** (1978) 35.

[78] J.-C. Novelli and J.-Y. Thibon, *Hopf Algebras of m-permutations, (m + 1)-ary trees, and m-parking functions*, arXiv:1403.5962.

[79] F. Cachazo and B. G. Umbert, *Connecting Scalar Amplitudes using The Positive Tropical Grassmannian*, arXiv:2205.0272.

[80] T. Wirtz, D. Waltner, M. Kieburg, and S. Kumar, *The correlated jacobi and the correlated cauchy–lorentz ensembles*, *Journal of Statistical Physics* **162** (nov, 2015) 495–521.

[81] S. Dutta and T. Faulkner, *A canonical purification for the entanglement wedge cross-section*, arXiv:1905.0057.

[82] C. Akers, T. Faulkner, S. Lin, and P. Rath, *Reflected entropy in random tensor networks*, *JHEP* **05** (2022) 162, [arXiv:2112.0912].

[83] C. Akers, T. Faulkner, S. Lin, and P. Rath, *The Page curve for reflected entropy*, *JHEP* **06** (2022) 089, [arXiv:2201.1173].

[84] C. Akers, T. Faulkner, S. Lin, and P. Rath, *Reflected entropy in random tensor networks II: a topological index from the canonical purification*, arXiv:2210.1500.